

Drivers of plant nutrient acquisition and allocation strategies and their influence  
on plant responses to environmental change

by

Evan A. Perkowski, B.S.

A Dissertation

In

Biological Sciences

Submitted to the Graduate Faculty  
of Texas Tech University in  
Partial Fulfillment of  
the Requirements for  
the Degree of

Doctor of Philosophy

Approved

Dr. Nicholas G. Smith  
Chair of Committee

Dr. Aimée T. Classen

Dr. Natasja van Gestel

Dr. Lindsey C. Slaughter

Dr. Dylan W. Schwilk

Dr. Mark Sheridan  
Dean of the Graduate School

May 2023

Copyright 2023, Evan A. Perkowski

## Acknowledgements

Placeholder for text

## Table of Contents

<b>Acknowledgements</b> . . . . .	ii
<b>Abstract</b> . . . . .	vi
<b>List of Tables</b> . . . . .	vii
<b>List of Figures</b> . . . . .	viii
<b>1. Introduction</b> . . . . .	1
<b>2. Structural carbon costs to acquire nitrogen are determined by nitrogen and light availability in two species with different nitrogen acquisition strategies</b> . . . . .	2
2.1 Introduction . . . . .	2
2.2 Methods . . . . .	6
2.2.1 <i>Experiment setup</i> . . . . .	6
2.2.2 <i>Plant measurements and calculations</i> . . . . .	7
2.2.3 <i>Statistical analyses</i> . . . . .	8
2.3 Results . . . . .	10
2.3.1 <i>Carbon costs to acquire nitrogen</i> . . . . .	10
2.3.2 <i>Whole plant nitrogen biomass</i> . . . . .	13
2.3.3 <i>Root carbon biomass</i> . . . . .	15
2.3.4 <i>Root nodule biomass</i> . . . . .	17
2.4 Discussion . . . . .	21
<b>3. Soil nitrogen availability modifies leaf nitrogen economies in mature temperate deciduous forests: a direct test of photosynthetic least-cost theory</b> . . . . .	29
3.1 Introduction . . . . .	29
3.2 Methods . . . . .	33
3.2.1 <i>Study site description</i> . . . . .	33
3.2.2 <i>Experimental design</i> . . . . .	34
3.2.3 <i>Leaf gas exchange and trait measurements</i> . . . . .	34
3.2.4 <i><math>A_{net}/C_i</math> curve-fitting and parameter estimation</i> . . . . .	37

3.2.5	<i>Proportion of leaf nitrogen allocated to photosynthesis and structure</i>	39
3.2.6	<i>Tradeoffs between nitrogen and water use</i>	40
3.2.7	<i>Soil nitrogen availability and pH</i>	41
3.2.8	<i>Statistical analyses</i>	43
3.3	Results	45
3.3.1	<i>Leaf N content</i>	45
3.3.2	<i>Net photosynthesis and leaf biochemistry</i>	48
3.3.3	<i>Leaf N allocation</i>	51
3.3.4	<i>Tradeoffs between nitrogen and water use</i>	54
3.4	Discussion	57
3.4.1	<i>Soil nitrogen availability modifies tradeoffs between nitrogen and water use</i>	58
3.4.2	<i>Soil pH did not modify tradeoffs between nitrogen and water usage</i>	60
3.4.3	<i>Species identity explains a large amount of variation in leaf and whole plant traits</i>	61
3.4.4	<i>Implications for photosynthetic least-cost theory model development</i>	62
3.4.5	<i>Conclusions</i>	64
4.	<b>The relative cost of resource use for photosynthesis drives variance in leaf nitrogen content across climate and soil resource availability gradients</b>	65
4.1	Introduction	65
4.2	Methods	66
4.3	Results	66
4.4	Discussion	66
5.	<b>Optimal resource investment to photosynthetic capacity maximizes nutrient allocation to whole plant growth under elevated CO<sub>2</sub></b>	67
5.1	Introduction	67

5.2	Methods . . . . .	67
5.3	Results . . . . .	67
5.4	Discussion . . . . .	67
6.	<b>Conclusions</b> . . . . .	68
	<b>References</b> . . . . .	69

## **Abstract**

## List of Tables

2.1	Analysis of variance results exploring species-specific effects of light availability, nitrogen fertilization, and their interactions on carbon costs to acquire nitrogen, whole-plant nitrogen biomass, and root carbon biomass . . . . .	11
2.2	Analysis of variance results exploring effects of light availability, nitrogen fertilization, and their interactions on <i>G. max</i> root nodule biomass and the ratio of root nodule biomass to root biomass* . .	18
2.3	Slopes of the regression line describing the relationship between each dependent variable and nitrogen fertilization at each light level*	19



## List of Figures

2.1	Relationships between soil nitrogen fertilization and light availability on carbon costs to acquire nitrogen in <i>G. hirsutum</i> and <i>G. max</i>	12
2.2	Relationships between soil nitrogen fertilization and light availability on whole-plant nitrogen biomass in <i>G. hirsutum</i> and <i>G. max</i>	14
2.3	Relationships between soil nitrogen fertilization and light availability on root carbon biomass in <i>G. hirsutum</i> and <i>G. max</i>	16
2.4	Effects of shade cover and nitrogen fertilization on root nodule biomass and the ratio of root nodule biomass to root biomass in <i>G. max</i>	20

**1**

**Chapter 1**

**2**

**Introduction**

3

## Chapter 2

4

5

6

# Structural carbon costs to acquire nitrogen are determined by nitrogen and light availability in two species with different nitrogen acquisition strategies

7

## 2.1 Introduction

8

9

10

11

12

13

14

15

16

17

18

19

20

21

22

23

Carbon and nitrogen cycles are tightly coupled in terrestrial ecosystems. This tight coupling influences photosynthesis (Walker et al. 2014; Rogers et al. 2017), net primary productivity (LeBauer and Treseder 2008; Thomas et al. 2013), decomposition (Cornwell et al. 2008; Bonan et al. 2013; Sulman et al. 2019), and plant resource competition (Gill and Finzi 2016; Xu-Ri and Prentice 2017). Terrestrial biosphere models are beginning to include connected carbon and nitrogen cycles to improve the realism of their simulations (Fisher et al. 2010; Brzostek et al. 2014; Wieder et al. 2015; Shi et al. 2016; Zhu et al. 2019). Simulations from these models indicate that coupling carbon and nitrogen cycles can drastically influence future biosphere-atmosphere feedbacks under global change, such as elevated carbon dioxide or nitrogen deposition (Thornton et al. 2007; Goll et al. 2012; Wieder et al. 2015; Wieder et al. 2019). Nonetheless, there are still limitations in our quantitative understanding of connected carbon and nitrogen dynamics (Thomas et al. 2015; Meyerholt et al. 2016; Rogers et al. 2017; Exbrayat et al. 2018; Shi et al. 2019), forcing models to make potentially unreliable assumptions.

24

25

26

Plant nitrogen acquisition is a process in terrestrial ecosystems by which carbon and nitrogen are tightly coupled (Vitousek and Howarth 1991; Delaire et al. 2005; Brzostek et al. 2014). Plants must allocate photosynthetically de-

27 rived carbon belowground to produce and maintain root systems or exchange with  
 28 symbiotic soil microbes in order to acquire nitrogen (Högberg et al. 2008; Hög-  
 29 berg et al. 2010). Thus, plants have an inherent carbon cost associated with  
 30 acquiring nitrogen, which can include both direct energetic costs associated with  
 31 nitrogen acquisition and indirect costs associated with building structures that  
 32 support nitrogen acquisition (Gutschick 1981; Rastetter et al. 2001; Vitousek  
 33 et al. 2002; Menge et al. 2008). Model simulations (Fisher et al. 2010; Brzostek  
 34 et al. 2014; Shi et al. 2016; Allen et al. 2020) and meta-analyses (Terrer et al.  
 35 2018) suggest that these carbon costs vary between species, particularly those  
 36 with different nitrogen acquisition strategies. For example, simulations using iter-  
 37 ations of the Fixation and Uptake of Nitrogen (FUN) model indicate that species  
 38 that acquire nitrogen from non-symbiotic active uptake pathways (e.g. mass flow)  
 39 generally have larger carbon costs to acquire nitrogen than species that acquire  
 40 nitrogen through symbiotic associations with nitrogen-fixing bacteria (Brzostek  
 41 et al. 2014; Allen et al. 2020).

42         Carbon costs to acquire nitrogen likely vary in response to changes in soil  
 43 nitrogen availability. For example, if the primary mode of nitrogen acquisition  
 44 is through non-symbiotic active uptake, then nitrogen availability could decrease  
 45 carbon costs to acquire nitrogen as a result of increased per-root nitrogen up-  
 46 take (Franklin et al. 2009; Wang et al. 2018). However, if the primary mode of  
 47 nitrogen acquisition is through symbiotic active uptake, then nitrogen availabil-  
 48 ity may incur additional carbon costs to acquire nitrogen if it causes microbial  
 49 symbionts to shift toward parasitism along the parasitism–mutualism continuum  
 50 (Johnson et al. 1997; Hoek et al. 2016; Friel and Friesen 2019) or if it reduces

the nitrogen acquisition capacity of a microbial symbiont (van Diepen et al. 2007; Soudzilovskaia et al. 2015; Muñoz et al. 2016). Species may respond to shifts in soil nitrogen availability by switching their primary mode of nitrogen acquisition to a strategy with lower carbon costs to acquire nitrogen in order to maximize the magnitude of nitrogen acquired from a belowground carbon investment and outcompete other individuals for soil resources (Rastetter et al. 2001; Menge et al. 2008).

Environmental conditions that affect demand to acquire nitrogen to support new and existing tissues could also be a source of variance in plant carbon costs to acquire nitrogen. For example, an increase in plant nitrogen demand could increase carbon costs to acquire nitrogen if this increases the carbon that must be allocated belowground to acquire a proportional amount of nitrogen (Kulmatiski et al. 2017; Noyce et al. 2019). This could be driven by a temporary state of diminishing return associated with investing carbon toward building and maintaining structures that are necessary to support enhanced nitrogen uptake, such as fine roots (Matamala and Schlesinger 2000; Norby et al. 2004; Arndal et al. 2018), mycorrhizal hyphae (Saleh et al. 2020), or root nodules (Parvin et al. 2020). Alternatively, if the environmental factor that increases plant nitrogen demand causes nitrogen to become more limiting in the system (e.g. atmospheric CO<sub>2</sub>; Luo et al. (2004), LeBauer and Treseder (2008), Vitousek et al. (2010), Liang et al. (2016)), species might switch their primary mode of nitrogen acquisition to a strategy with lower relative carbon costs to acquire nitrogen in order to gain a competitive advantage over species with either different or more limited modes of nitrogen acquisition (Ainsworth and Long 2005; Taylor and Menge 2018).

75        Using a plant economics approach, we examined the influence of plant  
76 nitrogen demand and soil nitrogen availability on plant carbon costs to acquire  
77 nitrogen. This was done by growing a species capable of forming associations  
78 with nitrogen-fixing bacteria (*Glycine max* L. (Merr)) and a species not capable  
79 of forming these associations (*Gossypium hirsutum* L.) under four levels of light  
80 availability (plant nitrogen demand proxy) and four levels of soil nitrogen fertil-  
81 ization (soil nitrogen availability proxy) in a full-factorial, controlled greenhouse  
82 experiment. We used this experimental set-up to test the following hypotheses:

- 83        1. An increase in plant nitrogen demand due to increasing light availability will  
84        increase carbon costs to acquire nitrogen through a proportionally larger  
85        increase in belowground carbon than whole-plant nitrogen acquisition. This  
86        will be the result of an increased investment of carbon toward belowground  
87        structures that support enhanced nitrogen uptake, but at a lower nitrogen  
88        return.
- 89        2. An increase in soil nitrogen availability will decrease carbon costs to acquire  
90        nitrogen as a result of increased per root nitrogen uptake in *G. hirsutum*.  
91        However, soil nitrogen availability will not affect carbon costs to acquire  
92        nitrogen in *G. max* because of the already high return of nitrogen supplied  
93        through nitrogen fixation.

## 94 2.2 Methods

### 95 2.2.1 *Experiment setup*

96 *Gossypium hirsutum* and *G. max* were planted in individual 3 liter pots  
97 (NS-300; Nursery Supplies, Orange, CA, USA) containing a 3:1 mix of unfertil-  
98 ized potting mix (Sungro Sunshine Mix #2, Agawam, MA, USA) to native soil  
99 extracted from an agricultural field most recently planted with *G. max* at the  
100 USDA-ARS Laboratory in Lubbock, TX, USA (33.59°N, -101.90°W). The field  
101 soil was classified as Amarillo fine sandy loam (75% sand, 10% silt, 15% clay).  
102 Upon planting, all *G. max* pots were inoculated with *Bradyrhizobium japonicum*  
103 (Verdesian N-Dure™ Soybean, Cary, NC, USA) to stimulate root nodulation. In-  
104 dividuals of both species were grown under similar, unshaded, ambient greenhouse  
105 conditions for 2 weeks to germinate and begin vegetative growth. Three blocks  
106 were set up in the greenhouse, each containing four light treatments created us-  
107 ing shade cloth that reduced incoming radiation by either 0 (full sun), 30, 50,  
108 or 80%. Two weeks post-germination, individuals were randomly placed in the  
109 four light treatments in each block. Individuals received one of four nitrogen fer-  
110 tilization doses as 100ml of a modified Hoagland solution (Hoagland and Arnon  
111 1950) equivalent to either 0, 70, 210, or 630 ppm N twice per week within each  
112 light treatment. Nitrogen fertilization doses were received as topical agents to  
113 the soil surface. Each Hoagland solution was modified to keep concentrations of  
114 other macro- and micronutrients equivalent (Supplementary Table S1). Plants  
115 were routinely well watered to eliminate water stress.

## 116 2.2.2 *Plant measurements and calculations*

117 Each individual was harvested after 5 weeks of treatment, and biomass  
 118 was separated by organ type (leaves, stems, and roots). Nodules on *G. max*  
 119 roots were also harvested. With the exception of the 0% shade cover and 630  
 120 ppm N treatment combination, all treatment combinations in both species had  
 121 lower average dry biomass:pot volume ratios than the 1:1 ratio recommended by  
 122 Poorter et al. (2012) to minimize the likelihood of pot volume-induced growth  
 123 limitation (Supplementary Tables S2, S3; Supplementary Fig. S1). All harvested  
 124 material was dried, weighed, and ground by organ type. Carbon and nitrogen  
 125 content ( $\text{g g}^{-1}$ ) was determined by subsampling from ground and homogenized  
 126 biomass of each organ type using an elemental analyzer (Costech 4010; Costech,  
 127 Inc., Valencia, CA, USA). We scaled these values to total leaf, stem, and root  
 128 carbon and nitrogen biomass (g) by multiplying dry biomass of each organ type  
 129 by carbon or nitrogen content of each corresponding organ type. Whole-plant  
 130 nitrogen biomass (g) was calculated as the sum of total leaf (g), stem (g), and  
 131 root (g) nitrogen biomass. Root nodule carbon biomass was not included in the  
 132 calculation of root carbon biomass; however, relative plant investment toward root  
 133 or root nodule standing stock was estimated as the ratio of root biomass to root  
 134 nodule biomass ( $\text{g g}^{-1}$ ), following similar metrics to those adopted by Dovrat et al.  
 135 (2018) and Dovrat et al. (2020).

136 Carbon costs to acquire nitrogen ( $\text{gC gN}^{-1}$ ) were estimated as the ratio of  
 137 total root carbon biomass (gC) to whole-plant nitrogen biomass (gN). This cal-  
 138 culation quantifies the relationship between carbon spent on nitrogen acquisition  
 139 and whole-plant nitrogen acquisition by using root carbon biomass as a proxy for



140 estimating the magnitude of carbon allocated toward nitrogen acquisition. This  
 141 calculation therefore assumes that the magnitude of root carbon standing stock is  
 142 proportional to carbon transferred to root nodules or mycorrhizae, or lost through  
 143 root exudation or turnover. This assumption has been supported in species that  
 144 associate with ectomycorrhizal fungi (Hobbie 2006; Hobbie and Hobbie 2008), but  
 145 is less clear in species that acquire nitrogen through non-symbiotic active uptake  
 146 or symbiotic nitrogen fixation. It is also unclear whether relationships between  
 147 root carbon standing stock and carbon transfer to root nodules are similar in mag-  
 148 nitude to carbon lost through exudation or when allocated toward other active  
 149 uptake pathways. Thus, because of the way we performed our measurements, our  
 150 proximal values of carbon costs to acquire nitrogen are underestimates.

### 151 2.2.3 *Statistical analyses*

152 We explored the effects of light and nitrogen availability on carbon costs to  
 153 acquire nitrogen using separate linear mixed-effects models for each species. Mod-  
 154 els included shade cover, nitrogen fertilization, and interactions between shade  
 155 cover and nitrogen fertilization as continuous fixed effects, and also included block  
 156 as a random intercept term. Three separate models for each species were built  
 157 with this independent variable structure for three different dependent variables: (i)  
 158 carbon costs to acquire nitrogen ( $\text{gC gN}^{-1}$ ); (ii) whole-plant nitrogen biomass (de-  
 159 nominator of carbon cost to acquire nitrogen;  $\text{gN}$ ); and (iii) root carbon biomass  
 160 (numerator of carbon cost to acquire nitrogen;  $\text{gC}$ ). We constructed two additional  
 161 models for *G. max* with the same model structure described above to investigate  
 162 the effects of light availability and nitrogen fertilization on root nodule biomass

163 (g) and the ratio of root nodule biomass to root biomass (unitless).

164 We used Shapiro–Wilk tests of normality to determine whether species-  
 165 specific linear mixed-effects model residuals followed a normal distribution. None  
 166 of our models satisfied residual normality assumptions when models were fit using  
 167 untransformed data (Shapiro–Wilk:  $P < 0.05$  in all cases). We attempted to satisfy  
 168 residual normality assumptions by first fitting models using dependent variables  
 169 that were natural-log transformed. If residual normality assumptions were still  
 170 not met (Shapiro–Wilk:  $P < 0.05$ ), then models were fit using dependent variables  
 171 that were square root transformed. All residual normality assumptions were satis-  
 172 fied when models were fit with either a natural-log or square root transformation  
 173 (Shapiro–Wilk:  $P > 0.05$  in all cases). Specifically, we natural-log transformed *G.*  
 174 *hirsutum* carbon costs to acquire nitrogen and *G. hirsutum* whole-plant nitrogen  
 175 biomass. We also square root transformed *G. max* carbon costs to acquire nitro-  
 176 gen, *G. max* whole-plant nitrogen biomass, root carbon biomass in both species,  
 177 *G. max* root nodule biomass, and the *G. max* ratio of root nodule biomass to root  
 178 biomass. We used the ‘lmer’ function in the ‘lme4’ R package (Bates et al. 2015)  
 179 to fit each model and the ‘Anova’ function in the ‘car’ R package (Fox and Weis-  
 180 berg 2019) to calculate Wald’s  $\chi^2$  to determine the significance ( $\alpha = 0.05$ ) of each  
 181 fixed effect coefficient. Finally, we used the ‘emmeans’ R package (Lenth 2019)  
 182 to conduct post-hoc comparisons of our treatment combinations using Tukey’s  
 183 tests. Degrees of freedom for all Tukey’s tests were approximated using the Ken-  
 184 ward–Roger approach (Kenward and Roger 1997). All analyses and plots were  
 185 conducted in R version 4.0.1 (R Core Team 2021).

## 186 2.3 Results

### 187 2.3.1 *Carbon costs to acquire nitrogen*

188        Carbon costs to acquire nitrogen in *G. hirsutum* increased with increasing  
189 light availability ( $P < 0.001$ ; Table 1; Fig. 1) and decreased with increasing nitrogen  
190 fertilization ( $P < 0.001$ ; Table 1; Fig. 1). There was no interaction between light  
191 availability and nitrogen fertilization ( $P = 0.486$ ; Table 2.1; Fig. 2.1).

192        Carbon costs to acquire nitrogen in *G. max* also increased with increasing  
193 light availability ( $P < 0.001$ ; Table 1; Fig. 1) and decreased with increasing nitrogen  
194 fertilization ( $P < 0.001$ ; Table 1; Fig. 1). There was no interaction between light  
195 availability and nitrogen fertilization ( $P = 0.261$ ; Table 2.1; Fig. 2.1).

**Table 2.1.** Analysis of variance results exploring species-specific effects of light availability, nitrogen fertilization, and their interactions on carbon costs to acquire nitrogen, whole-plant nitrogen biomass, and root carbon biomass

		Carbon costs to acquire nitrogen			Whole-plant nitrogen biomass			Root carbon biomass		
	df	Coefficient	$\chi^2$	<i>P</i> -value	Coefficient	$\chi^2$	<i>P</i> -value	Coefficient	$\chi^2$	<i>P</i> -value
<i>G. hirsutum</i>										
Intercept		1.594	-	-	-3.232	-	-	0.432	-	-
Light (L)	1	-1.09E-02	56.494	< <b>0.001</b>	-6.41E-03	91.275	< <b>0.001</b>	-2.62E-03	169.608	< <b>0.001</b>
Nitrogen (N)	1	-1.34E-03	54.925	< <b>0.001</b>	1.83E-03	118.784	< <b>0.001</b>	1.15E-04	2.901	<i>0.089</i>
L*N	1	3.88E-06	0.485	0.486	-1.34E-05	10.721	<b>0.001</b>	-1.67E-06	3.140	<i>0.076</i>
<i>G. max</i>										
Intercept		1.877	-	-	0.239	-	-	0.438	-	-
Light (L)	1	-7.67E-03	174.156	< <b>0.001</b>	-6.72E-04	39.799	< <b>0.001</b>	-2.55E-03	194.548	< <b>0.001</b>
Nitrogen (N)	1	-2.35E-04	21.948	< <b>0.001</b>	1.55E-04	70.771	< <b>0.001</b>	2.52E-04	19.458	< <b>0.001</b>
L*N	1	-2.89E-06	1.262	0.261	-6.32E-07	1.435	0.231	-3.16E-06	10.803	<b>0.001</b>

\*Significance determined using Wald's  $\chi^2$  tests ( $P=0.05$ ).  $P$ -values<0.05 are in bold and marginally insignificant  $P$ -values between 0.050 and 0.100 are italicized. Negative coefficients for light treatments indicate a positive effect of increasing light availability on all response variables, as light availability is treated as percent shade cover in all linear mixed-effects models.

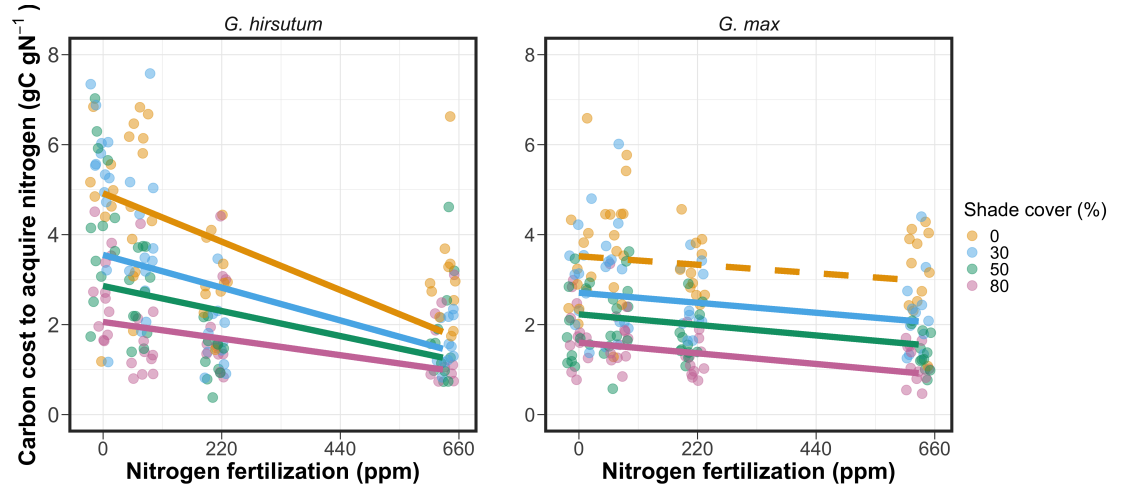


**Figure 2.1.** Relationships between soil nutrient fertilization and light availability on carbon costs to acquire nitrogen in *G. hirsutum* and *G. max*. Nitrogen fertilization treatments are represented on the x-axis. Shade cover treatments are represented through colored points and trendlines. Trendlines were created by back-transforming marginal mean slopes and intercepts from species-specific linear mixed-effects models. These values were calculated using the ‘emtrends’ and ‘emmeans’ functions in the ‘emmeans’ R package (Lenth, 2019). Points are jittered for visibility. Yellow points and trendlines represent the 0% shade cover treatment, blue points and trendlines represent the 30% shade cover treatment, green points and trendlines represent the 50% shade cover treatment, and purple points and trendlines represent the 80% shade cover treatment. Solid trendlines indicate slopes that are significantly different from zero (Tukey:  $P < 0.05$ ), while dashed trendlines indicate slopes that are not statistically different from zero.

**196** 2.3.2 *Whole plant nitrogen biomass*

**197** Whole-plant nitrogen biomass in *G. hirsutum* was driven by an interaction  
**198** between light availability and nitrogen fertilization ( $P=0.001$ ; Table 1; Fig. 2).  
**199** This interaction indicated a greater stimulation of whole-plant nitrogen biomass  
**200** by nitrogen fertilization as light levels increased (Table 2.1; Fig. 2.2).

**201** Whole-plant nitrogen biomass in *G. max* increased with increasing light  
**202** availability ( $P<0.001$ ) and nitrogen fertilization ( $P<0.001$ ), with no interaction  
**203** between light availability and nitrogen fertilization ( $P=0.231$ ; Table 2.1; Fig. 2.2).

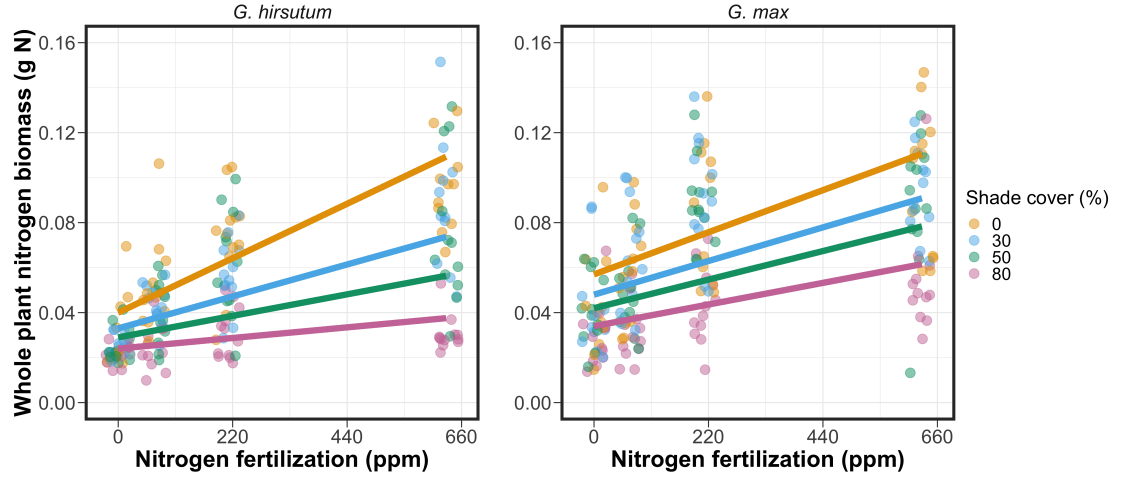


**Figure 2.2.** Relationships between soil nutrient fertilization and light availability on whole-plant nitrogen biomass in *G. hirsutum* and *G. max*. Whole-plant nitrogen biomass is the denominator of the carbon cost to acquire nitrogen calculation. Nitrogen fertilization treatments are represented on the x-axis. Shade cover treatments are represented through colored points and trendlines. Trendlines were created by back-transforming marginal mean slopes and intercepts from species-specific linear mixed-effects models. These values were calculated using the ‘emtrends’ and ‘emmeans’ functions in the ‘emmeans’ R package (Lenth 2019). Points are jittered for visibility. Yellow points and trendlines represent the 0% shade cover treatment, blue points and trendlines represent the 30% shade cover treatment, green points and trendlines represent the 50% shade cover treatment, and purple points and trendlines represent the 80% shade cover treatment. Solid trendlines indicate slopes that are significantly different from zero (Tukey:  $P < 0.05$ ), while dashed trendlines indicate slopes that are not statistically different from zero.

### 204 2.3.3 *Root carbon biomass*

205           Root carbon biomass in *G. hirsutum* significantly increased with increasing  
 206 light availability ( $P < 0.001$ ; Table 1; Fig. 3) and marginally increased with nitro-  
 207 gen fertilization ( $P = 0.089$ ; Table 1; Fig. 3). There was also a marginal interaction  
 208 between light availability and nitrogen fertilization ( $P = 0.076$ ; Table 1), driven by  
 209 an increase in the positive response of root carbon biomass to increasing nitrogen  
 210 fertilization as light availability increased. This resulted in significantly positive  
 211 trends between root carbon biomass and nitrogen fertilization in the two highest  
 212 light treatments (Tukey:  $P < 0.05$  in both cases; Table 2.3; Fig. 2.3) and no effect  
 213 of nitrogen fertilization in the two lowest light treatments (Tukey:  $P > 0.05$  in both  
 214 cases; Table 3; Fig. 3).

215           There was an interaction between light availability and nitrogen fertiliza-  
 216 tion on root carbon biomass in *G. max* ( $P = 0.001$ ; Table 1; Fig. 3). Post-hoc  
 217 analyses indicated that the positive effects of nitrogen fertilization on *G. max*  
 218 root carbon biomass increased with increasing light availability (Table 3; Fig.  
 219 3). There were also positive individual effects of increasing nitrogen fertilization  
 220 ( $P < 0.001$ ) and light availability ( $P < 0.001$ ) on *G. max* root carbon biomass (Table  
 221 1; Fig. 2.3).



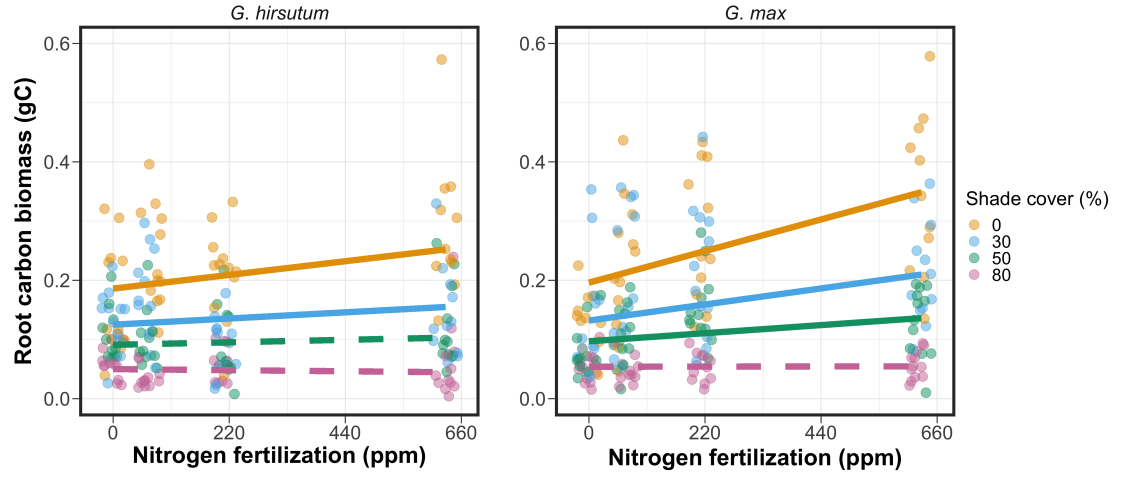


**Figure 2.3.** Relationships between soil nutrient fertilization and light availability on root carbon biomass in *G. hirsutum* and *G. max*. Root carbon biomass is the numerator of the carbon cost to acquire nitrogen calculation. Nitrogen fertilization treatments are represented on the x-axis. Shade cover treatments are represented through colored points and trendlines. Trendlines were created by back-transforming marginal mean slopes and intercepts from species-specific linear mixed-effects models. These values were calculated using the ‘emtrends’ and ‘emmeans’ functions in the ‘emmeans’ R package (Lenth 2019). Points are jittered for visibility. Yellow points and trendlines represent the 0% shade cover treatment, blue points and trendlines represent the 30% shade cover treatment, green points and trendlines represent the 50% shade cover treatment, and purple points and trendlines represent the 80% shade cover treatment. Solid trendlines indicate slopes that are significantly different from zero (Tukey:  $P < 0.05$ ), while dashed trendlines indicate slopes that are not statistically different from zero.

**222** 2.3.4 *Root nodule biomass*

**223** Root nodule biomass in *G. max* increased with increasing light availability  
**224** ( $P < 0.001$ ; Table 2; Fig. 4A) and decreased with increasing nitrogen fertilization  
**225** ( $P < 0.001$ ; Table 2; Fig. 4A). There was no interaction between nitrogen fertiliza-  
**226** tion and light availability ( $P = 0.133$ ; Table 2; Fig. 4A). The ratio of root nodule  
**227** biomass to root biomass did not change in response to light availability ( $P = 0.481$ ;  
**228** Table 2; Fig. 4B) but decreased with increasing nitrogen fertilization ( $P < 0.001$ ;  
**229** Table 2; Fig. 4B). There was no interaction between nitrogen fertilization and  
**230** light availability on the ratio of root nodule biomass to root biomass ( $P = 0.621$ ;  
**231** Table 2; Fig. 4B).

**Table 2.2.** Analysis of variance results exploring effects of light availability, nitrogen fertilization, and their interactions on *G. max* root nodule biomass and the ratio of root nodule biomass to root biomass\*

	Nodule biomass				Nodule biomass: root biomass		
	df	Coefficient	$\chi^2$	<i>P</i> -value	Coefficient	$\chi^2$	<i>P</i> -value
Intercept		0.302	-	-	0.448	-	-
Light (L)	1	-1.81E-03	72.964	<b>&lt;0.001</b>	-8.76E-05	0.496	0.481
Nitrogen (N)	1	-2.83E-04	115.377	<b>&lt;0.001</b>	-5.09E-04	156.476	<b>&lt;0.001</b>
L*N	1	1.14E-06	2.226	0.133	-7.30E-07	0.244	0.621

\*Significance determined using Wald's  $\chi^2$  tests ( $\alpha=0.05$ ). *P*-values less than 0.05 are in bold. Negative coefficients for light treatments indicate a positive effect of increasing light availability on all response variables, as light availability is treated as percent shade cover in all linear mixed-effects models. Root nodule biomass and nodule biomass: root biomass models were only constructed for *G. max* because *G. hirsutum* was not inoculated with *B. japonicum* and is not capable of forming root nodules.

**Table 2.3.** Slopes of the regression line describing the relationship between each dependent variable and nitrogen fertilization at each light level\*

Shade cover	Carbon cost to acquire nitrogen	Whole-plant nitrogen biomass	Root carbon biomass	Root nodule biomass	Nodule biomass root biomass
<i>G. hirsutum</i>					
0%	<b>-1.34E-03<sup>a</sup></b>	<b>1.83E-03<sup>a</sup></b>	<b>1.15E-04<sup>b</sup></b>	-	-
30%	<b>-1.22E-03<sup>a</sup></b>	<b>1.43E-03<sup>a</sup></b>	<b>1.17E-04<sup>b</sup></b>	-	-
50%	<b>-1.14E-03<sup>a</sup></b>	<b>1.17E-03<sup>a</sup></b>	3.12E-05 <sup>b</sup>	-	-
80%	<b>-1.02E-03<sup>a</sup></b>	<b>7.66E-04<sup>a</sup></b>	-1.89E-06 <sup>b</sup>	-	-
<i>G. max</i>					
0%	-2.35E-04 <sup>b</sup>	<b>1.55E-05<sup>b</sup></b>	<b>2.51E-04<sup>b</sup></b>	<b>-2.83E-04<sup>b</sup></b>	<b>-5.09E-04<sup>b</sup></b>
30%	<b>-3.22E-04<sup>b</sup></b>	<b>1.35E-05<sup>b</sup></b>	<b>1.57E-04<sup>b</sup></b>	<b>-2.49E-04<sup>b</sup></b>	<b>-5.31E-04<sup>b</sup></b>
50%	<b>-3.80E-04<sup>b</sup></b>	<b>1.23E-05<sup>b</sup></b>	<b>9.37E-05<sup>b</sup></b>	<b>-2.26E-04<sup>b</sup></b>	<b>-5.45E-04<sup>b</sup></b>
80%	<b>-4.66E-04<sup>b</sup></b>	<b>1.04E-05<sup>b</sup></b>	-9.95E-07 <sup>b</sup>	<b>-1.92E-04<sup>b</sup></b>	<b>-5.67E-04<sup>b</sup></b>

\*Slopes represent estimated marginal mean slopes from linear mixed-effects models described in the Methods. Slopes were calculated using the ‘emmeans’ R package (Lenth 2019). Superscripts indicate slopes fit to natural-log (<sup>a</sup>) or square root (<sup>b</sup>) transformed data. Slopes statistically different from zero (Tukey:  $P < 0.05$ ) are indicated in bold. Marginally significant slopes (Tukey:  $0.05 < P < 0.1$ ) are italicized.

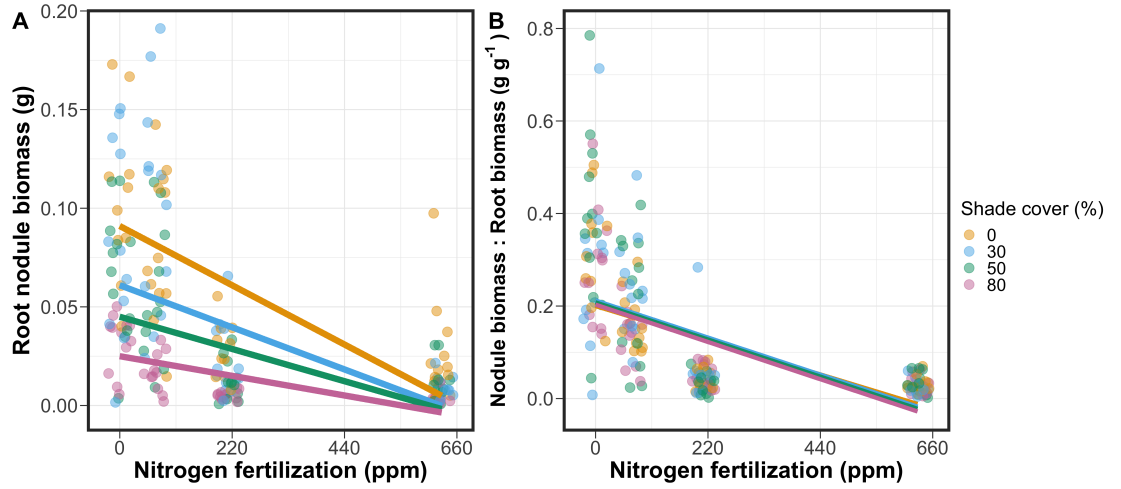


**Figure 2.4.** Effects of shade cover and nitrogen fertilization on root nodule biomass (A) and the ratio of root nodule biomass to root biomass (B) in *G. max*. Nitrogen fertilization treatments are represented on the x-axis. Shade cover treatments are represented through colored points and trendlines. Trendlines were created by back-transforming marginal mean slopes and intercepts from species-specific linear mixed-effects models. These values were calculated using the ‘emtrends’ and ‘emmeans’ functions in the ‘emmeans’ R package (Lenth, 2019). Points are jittered for visibility. Yellow points and trendlines represent the 0% shade cover treatment, blue points and trendlines represent the 30% shade cover treatment, green points and trendlines represent the 50% shade cover treatment, and purple points and trendlines represent the 80% shade cover treatment. Solid trendlines indicate slopes that are significantly different from zero (Tukey:  $P < 0.05$ ), while dashed trendlines indicate slopes that are not statistically different from zero.

## 232 2.4 Discussion

233 In this chapter, we determined the effects of light availability and soil ni-  
 234 trogen fertilization on root mass carbon costs to acquire nitrogen in *G. hirsutum*  
 235 and *G. max*. In support of our hypotheses, we found that carbon costs to acquire  
 236 nitrogen generally increased with increasing light availability and decreased with  
 237 increasing soil nitrogen fertilization in both species. These findings suggest that  
 238 carbon costs to acquire nitrogen are determined by factors that influence plant  
 239 nitrogen demand and soil nitrogen availability. In contrast to our second hypothe-  
 240 sis, root nodulation data suggested that *G. max* and *G. hirsutum* achieved similar  
 241 directional carbon cost responses to nitrogen fertilization despite a likely shift in  
 242 *G. max* allocation from nodulation to root biomass along the nitrogen fertilization  
 243 gradient (Fig. 2.4B).

244 Both *G. max* and *G. hirsutum* experienced an increase in carbon costs to  
 245 acquire nitrogen due to increasing light availability. These patterns were driven by  
 246 a larger increase in root carbon biomass than whole-plant nitrogen biomass. In-  
 247 creases in root carbon biomass due to factors that increase plant nitrogen demand  
 248 are a commonly observed pattern, as carbon allocated belowground provides sub-  
 249 strate needed to produce and maintain structures that satisfy aboveground plant  
 250 nitrogen demand (Nadelhoffer and Raich 1992; Giardina et al. 2005; Raich et al.  
 251 2014). Our findings suggest that plants allocate relatively more carbon for acquir-  
 252 ing nitrogen when demand increases over short temporal scales, which may cause  
 253 a temporary state of diminishing return due to asynchrony between belowground  
 254 carbon and whole-plant nitrogen responses to plant nitrogen demand (Kulmatiski  
 255 et al. 2017; Noyce et al. 2019). These responses might be attributed to a temporal

lag associated with producing structures that enhance nitrogen acquisition. For example, fine roots (Matamala and Schlesinger 2000; Norby et al. 2004; Arndal et al. 2018) and root nodules (Parvin et al. 2020) take time to build and first require the construction of coarse roots. Thus, full nitrogen returns from these investments may not occur immediately (Kayler et al. 2010; Kayler et al. 2017), and may vary by species acquisition strategy. We speculate that increases in nitrogen acquisition from a given carbon investment may occur beyond the 5 week scope of this experiment. A similar study conducted over a longer temporal scale would address this.

Increasing soil nitrogen fertilization generally decreased carbon costs to acquire nitrogen in both species. These patterns were driven by a larger increase in whole-plant nitrogen biomass than root carbon biomass. In *G. hirsutum*, reductions in carbon costs to acquire nitrogen may have been due to an increase in per-root nitrogen uptake, allowing individuals to maximize the amount of nitrogen acquired from a belowground carbon investment. Interestingly, increased soil nitrogen fertilization increased whole-plant nitrogen biomass in *G. max* despite reductions in root nodule biomass that likely reduced the nitrogen-fixing capacity of *G. max* (Andersen et al. 2005; Muñoz et al. 2016). While reductions in root nodulation due to increased soil nitrogen availability are commonly observed (Gibson and Harper 1985; Fujikake et al. 2003), our responses were observed in tandem with increased root carbon biomass, implying that *G. max* shifted relative carbon allocation from nitrogen fixation to soil nitrogen acquisition (Markham and Zekveld 2007; Dovrat et al. 2020). This was likely because there was a reduction in the carbon cost advantage of acquiring fixed nitrogen relative to soil nitrogen, and

280 suggests that species capable of associating with symbiotic nitrogen-fixing bacte-  
281 ria shift their relative nitrogen acquisition pathway to optimize nitrogen uptake  
282 (Rastetter et al. 2001). Future studies should further investigate these patterns  
283 with a larger quantity of phylogenetically related species, or different varieties  
284 of a single species that differ in their ability to form associations with symbiotic  
285 nitrogen-fixing bacteria to more directly test the impact of nitrogen fixation on  
286 the patterns observed in this study.

287         Carbon costs to acquire nitrogen are subsumed in the general discussion of  
288 economic analogies to plant resource uptake (Bloom et al. 1985; Rastetter et al.  
289 2001; Vitousek et al. 2002; Phillips et al. 2013; Terrer et al. 2018; Henneron et al.  
290 2020). Despite this, terrestrial biosphere models rarely include these carbon costs  
291 within their framework for predicting plant nitrogen uptake. There is currently  
292 one plant resource uptake model, FUN, that quantitatively predicts carbon costs  
293 to acquire nitrogen within a framework for predicting plant nitrogen uptake for  
294 different nitrogen acquisition strategies (Fisher et al. 2010; Brzostek et al. 2014)

295         (Fisher et al. 2010; Brzostek et al. 2014). Iterations of FUN are currently  
296 coupled to two terrestrial biosphere models: the Community Land Model 5.0 and  
297 the Joint UK Land Environment Simulator (Shi et al. 2016; Lawrence et al.  
298 2019; Clark et al. 2011). Recent work suggests that coupling FUN to CLM 5.0  
299 caused a large overprediction of plant nitrogen uptake associated with nitrogen  
300 fixation (Davies-Barnard et al. 2020). Thus, empirical data from manipulative  
301 experiments that explicitly quantify carbon costs to acquire nitrogen in species  
302 capable of associating with nitrogen-fixing bacteria across different environmental  
303 contexts is an important step toward identifying potential biases in models such



304 as FUN.

305       Our findings broadly support the FUN formulation of carbon costs to ac-  
 306 quire nitrogen in response to soil nitrogen availability. FUN calculates carbon  
 307 costs to acquire nitrogen based on the sum of carbon costs to acquire nitrogen via  
 308 nitrogen fixation, mycorrhizal active uptake, non-mycorrhizal active uptake, and  
 309 retranslocation

310       (Fisher et al. 2010; Brzostek et al. 2014). Carbon costs to acquire nitrogen  
 311 via mycorrhizal or non-mycorrhizal active uptake pathways are derived as a func-  
 312 tion of nitrogen availability, root biomass, and two parameterized values based on  
 313 nitrogen acquisition strategy (Brzostek et al. 2014). Due to this, FUN simulates  
 314 a net decrease in carbon costs to acquire nitrogen with increasing nitrogen avail-  
 315 ability for mycorrhizal and non-mycorrhizal active uptake pathways, assuming  
 316 constant root biomass. This was a pattern we observed in *G. hirsutum* regardless  
 317 of light availability. In contrast, FUN would not simulate a net change in carbon  
 318 costs to acquire nitrogen via nitrogen fixation due to nitrogen availability. This  
 319 is because carbon costs to acquire nitrogen via nitrogen fixation are derived from  
 320 a well-established function of soil temperature, which is independent of soil ni-  
 321 trogen availability (Houlton et al. 2008; Fisher et al. 2010). We observed a net  
 322 reduction in carbon costs to acquire nitrogen in *G. max*, except when individuals  
 323 were grown under 0% shade cover (Fig. 1). While a net reduction of carbon costs  
 324 in response to nitrogen fertilization runs counter to nitrogen fixation carbon costs  
 325 simulated by FUN, these patterns were likely because *G. max* individuals switched  
 326 their primary mode of nitrogen acquisition from symbiotic nitrogen fixation to a  
 327 non-symbiotic active uptake pathway (Fig. 4B).

328           It should be noted that the metric used in this study to determine carbon  
 329 costs to acquire nitrogen has several limitations. Most notably, this metric uses  
 330 root carbon biomass as a proxy for estimating the amount of carbon spent on  
 331 nitrogen acquisition. While it is true that most carbon allocated belowground  
 332 has at least an indirect structural role in acquiring soil resources, it remains un-  
 333 clear whether this assumption holds true for species that acquire nitrogen via  
 334 symbiotic nitrogen fixation. We also cannot quantify carbon lost through root  
 335 exudates or root turnover, which may increase due to factors that increase plant  
 336 nitrogen demand (Tingey et al. 2000; Phillips et al. 2011), and can increase the  
 337 magnitude of available nitrogen from soil organic matter through priming effects  
 338 on soil microbial communities (Usselman et al. 2000; Bengtson et al. 2012). It  
 339 is also not clear whether these assumptions hold under all environmental condi-  
 340 tions, such as those that shift belowground carbon allocation toward a different  
 341 mode of nitrogen acquisition (Taylor and Menge 2018; Friel and Friesen 2019)  
 342 or between species with different acquisition strategies. In this study, increasing  
 343 soil nitrogen fertilization increased carbon investment to roots relative to carbon  
 344 transferred to root nodules (Fig. 4B). By assuming that carbon allocated to root  
 345 carbon was proportional to carbon allocated to root nodules across all treatment  
 346 combinations, these observed responses to soil nitrogen fertilization were likely  
 347 to be overestimated in *G. max*. We encourage future research to quantify these  
 348 carbon fates independently.

349           Researchers conducting pot experiments must carefully choose pot volume  
 350 to minimize the likelihood of pot volume-induced growth limitation (Poorter et al.  
 351 2012). Poorter et al. (2012) indicate that researchers are likely to avoid growth

352 limitations associated with pot volume if measurements are collected when the  
 353 plant biomass:pot volume ratio is less than 1 g L<sup>-1</sup>. In this experiment, all treat-  
 354 ment combinations in both species had biomass:pot volume ratios less than 1 g  
 355 L<sup>-1</sup> except for *G. max* and *G. hirsutum* that were grown under 0% shade cover  
 356 and had received 630 ppm N. Specifically, *G. max* and *G. hirsutum* had average  
 357 respective biomass:pot volume ratios of  $1.24 \pm 0.07$  g L<sup>-1</sup> and  $1.34 \pm 0.13$  g L<sup>-1</sup>, when  
 358 grown under 0% shade cover and received 630 ppm N (Supplementary Tables S2,  
 359 S3; Supplementary Fig. S1). If growth in this treatment combination was limited  
 360 by pot volume, then individuals may have had larger carbon costs to acquire ni-  
 361 trogen than would be expected if they were grown in larger pots. This pot volume  
 362 induced growth limitation could cause a reduction in per-root nitrogen uptake as-  
 363 sociated with more densely packed roots, which could reduce the positive effect  
 364 of nitrogen fertilization on whole-plant nitrogen biomass relative to root carbon  
 365 biomass (Poorter et al. 2012).

366 Growth limitation associated with pot volume provides a possible explana-  
 367 tion for the marginally insignificant effect of increasing nitrogen fertilization on *G.*  
 368 *max* carbon costs to acquire nitrogen when grown under 0% shade cover (Table  
 369 3; Fig. 1). This is because the regression line describing the relationship between  
 370 carbon costs to acquire nitrogen and nitrogen fertilization in *G. max* grown un-  
 371 der 0% shade cover would have flattened if growth limitation had caused larger  
 372 than expected carbon costs to acquire nitrogen in the 0% shade cover, 630 ppm  
 373 N treatment combination. This may have been exacerbated by the fact that *G.*  
 374 *max* likely shifted relative carbon allocation from nitrogen fixation to soil nitrogen  
 375 acquisition, which could have increased the negative effect of more densely packed

376 roots on nitrogen uptake. These patterns could have also occurred in *G. hirsutum*  
377 grown under 0% shade cover; however, there was no change in the effect of nitro-  
378 gen fertilization on *G. hirsutum* carbon costs to acquire nitrogen grown under 0%  
379 shade cover relative to other shade cover treatments. Regardless, the possibility  
380 of growth limitation due to pot volume suggests that effects of increasing nitro-  
381 gen fertilization on carbon costs to acquire nitrogen in both species grown under  
382 0% shade cover could have been underestimated. Follow-up studies using a simi-  
383 lar experimental design with a larger pot volume would be necessary in order to  
384 determine whether these patterns were impacted by pot volume-induced growth  
385 limitation.

386         In conclusion, this study provides empirical evidence that carbon costs to  
387 acquire nitrogen are influenced by light availability and soil nitrogen fertilization  
388 in a species capable of acquiring nitrogen via symbiotic nitrogen fixation and a  
389 species not capable of forming such associations. We show that carbon costs to  
390 acquire nitrogen generally increase with increasing light availability and decrease  
391 with increasing nitrogen fertilization. This study provides important empirical  
392 data needed to evaluate the formulation of carbon costs to acquire nitrogen in  
393 terrestrial biosphere models, particularly carbon costs to acquire nitrogen that  
394 are associated with symbiotic nitrogen fixation. Our findings broadly support  
395 the general formulation of these carbon costs in the FUN biogeochemical model  
396 in response to shifts in nitrogen availability. However, there is a need for future  
397 studies to explicitly quantify carbon costs to acquire nitrogen under different en-  
398 vironmental contexts, over longer temporal scales, and using larger selections of  
399 phylogenetically related species. In addition, we suggest that future studies mini-

**400** mize the limitations associated with the metric used here by explicitly measuring  
**401** belowground carbon fates independently.

402

## Chapter 3

403 **Soil nitrogen availability modifies leaf nitrogen economies in mature**  
 404 **temperate deciduous forests: a direct test of photosynthetic least-cost**  
 405 **theory**

### 406 3.1 Introduction

407       Photosynthesis represents the largest carbon flux between the atmosphere  
 408 and land surface (IPCC 2021), and plays a central role in biogeochemical cycling  
 409 at multiple spatial and temporal scales (Vitousek and Howarth 1991; LeBauer and  
 410 Treseder 2008; Kaiser et al. 2015; Wieder et al. 2015). Therefore, carbon and  
 411 energy fluxes simulated by terrestrial biosphere models are sensitive to the formu-  
 412 lation of photosynthetic processes (Ziehn et al. 2011; Bonan et al. 2011; Booth  
 413 et al. 2012; Smith et al. 2016; Smith et al. 2017) and must be represented using  
 414 robust, empirically tested processes (Prentice et al. 2015; Wieder et al. 2019).  
 415 Current formulations of photosynthesis vary across terrestrial biosphere models  
 416 (Smith and Dukes 2013; Rogers et al. 2017), which causes variation in modeled  
 417 ecosystem processes (Knorr 2000; Knorr and Heimann 2001; Bonan et al. 2011;  
 418 Friedlingstein et al. 2014) and casts uncertainty on the ability of these models to  
 419 accurately predict terrestrial ecosystem responses and feedbacks to global change  
 420 (Zaehle et al. 2005; Schaefer et al. 2012; Davies-Barnard et al. 2020).

421       Terrestrial biosphere models commonly represent  $C_3$  photosynthesis through  
 422 variants of the Farquhar et al. (1980) biochemical model (Smith and Dukes 2013;  
 423 Rogers 2014; Rogers et al. 2017). This well-tested photosynthesis model es-  
 424 timates leaf-level carbon assimilation, or photosynthetic capacity, as a function  
 425 of the maximum rate of Ribulose-1,5-bisphosphate carboxylase-oxygenase (Ru-

426 bisco) carboxylation ( $V_{cmax}$ ) and the maximum rate of Ribulose-1,5-bisphosphate  
 427 (RuBP) regeneration ( $J_{max}$ ) (Farquhar et al. 1980). Many terrestrial biosphere  
 428 models predict these model inputs based on plant functional group specific linear  
 429 relationships between leaf nutrient content and  $V_{cmax}$  (Smith and Dukes 2013;  
 430 Rogers 2014; Rogers et al. 2017) under the tenet that a large fraction of leaf  
 431 nutrients, and nitrogen (N) in particular, are partitioned toward building and  
 432 maintaining enzymes that support photosynthetic capacity, such as Rubisco (Brix  
 433 1971; Gulmon and Chu 1981; Evans 1989; Kattge et al. 2009; Walker et al. 2014).  
 434 Terrestrial biosphere models also predict leaf nutrient content from soil nutrient  
 435 availability based on the assumption that increasing soil nutrients generally in-  
 436 creases leaf nutrients (Firn et al. 2019; Li et al. 2020; Liang et al. 2020) which, in  
 437 the case of N, generally corresponds with an increase in photosynthetic processes  
 438 (Li et al. 2020; Liang et al. 2020).

439       Recent work calls the generality of relationships between soil nutrient avail-  
 440 ability, leaf nutrient content, and photosynthetic capacity into question, suggest-  
 441 ing instead that leaf nutrients and photosynthetic capacity are better predicted as  
 442 an integrated product of aboveground climate, leaf traits, and soil nutrient avail-  
 443 ability, rather than soil nutrient availability alone (Dong et al. 2017; Dong et al.  
 444 2020; Dong et al. 2022; Firn et al. 2019; Smith et al. 2019; Peng et al. 2021).  
 445 It has been reasoned that this result is because plants allocate added nutrients to  
 446 growth and storage rather than alterations in leaf chemistry (Smith et al. 2019),  
 447 perhaps as a result of nutrient limitation of primary productivity (LeBauer and  
 448 Treseder 2008; Fay et al. 2015). Additionally, recent work suggests that relation-  
 449 ships between leaf nutrient content and photosynthesis vary across environments,

450 and that the proportion of leaf nutrient content allocated to photosynthetic tis-  
 451 sue varies over space and time with plant acclimation and adaptation responses  
 452 to light availability, vapor pressure deficit, soil pH, soil nutrient availability, and  
 453 environmental factors that influence leaf mass per area (Pons and Pearcy 1994;  
 454 Niinemets and Tenhunen 1997; Evans and Poorter 2001; Hikosaka and Shigeno  
 455 2009; Ghimire et al. 2017; Onoda et al. 2017; Luo et al. 2021). The use of linear  
 456 relationships between leaf nutrient content and  $V_{\text{max}}$  to predict photosynthetic  
 457 capacity, as commonly used in terrestrial biosphere models (Rogers 2014), is not  
 458 capable of detecting such responses.

459         Photosynthetic least-cost theory provides an alternative framework for un-  
 460 derstanding relationships between soil nutrient availability, leaf nutrient content,  
 461 and photosynthetic capacity (Harrison et al. 2021). Leveraging a two-input mi-  
 462 croeconomics approach (Wright et al. 2003), the theory posits that plants accli-  
 463 mate to a given environment by optimizing leaf photosynthesis rates at the lowest  
 464 summed cost of using nutrients and water (Prentice et al. 2014; Wang et al. 2017;  
 465 Smith et al. 2019; Paillassa et al. 2020). Across resource availability gradients,  
 466 the theory predicts that optimal photosynthetic rates can be achieved by trading  
 467 less efficient use of a resource that is less costly to acquire (or more abundant)  
 468 for more efficient use of a resource more costly to acquire (or less abundant). For  
 469 example, an increase in soil nutrient availability should reduce the cost of acquir-  
 470 ing and using nutrients (Bae et al. 2015; Eastman et al. 2021; Perkowski et al.  
 471 2021), which could increase leaf nutrient investments in photosynthetic proteins to  
 472 allow similar photosynthetic rates to be achieved with higher nutrient use (lower  
 473 nutrient use efficiency) but lower water use (greater water use efficiency). The



theory suggests similar tradeoffs in response to increasing soil pH (Paillassa et al. 2020), specifically, that increasing soil pH should reduce the cost of acquiring soil nutrients due to an increase in plant-available nutrient concentration (Paillassa et al. 2020; Dong et al. 2022). The theory is also capable of reconciling dynamic leaf nutrient-photosynthesis relationships at global scales (Luo et al. 2021).

Patterns expected from photosynthetic least-cost theory have recently received empirical support both in global environmental gradient (Smith et al. 2019; Paillassa et al. 2020; Luo et al. 2021; Querejeta et al. 2022; Westerland et al. 2023) and local manipulative invasion (Bialic-Murphy et al. 2021) studies. However, nutrient addition experiments that directly examine nutrient-water use tradeoffs expected from the theory are rare (Guerrieri et al. 2011), and only global gradient studies testing the theory have considered soil pH in their analyses. As a result, there is a need to use nutrient addition and soil pH manipulation experiments to test mechanisms driving responses predicted by the theory. Such experiments would also be useful to detect whether patterns expected from theory translate to finer spatial scales.

In this study, we measured leaf responses to soil N availability in five deciduous tree species growing in the upper canopy of mature closed canopy temperate forests in the northeastern United States. Soil N availability and pH were manipulated through a N-by-pH field manipulation experiment with treatments applied since 2011, eight years prior to measurement. Two different soil N treatments were applied to increase N availability with opposing effects on soil pH. An additional N-free acidifying treatment was expected to decrease soil pH. We hypothesized that increased soil N availability would enable plants to increase nutrient uptake

and create more photosynthetic enzymes per leaf, allowing similar photosynthetic rates achieved with lower leaf  $C_i:C_a$  and increased leaf N content allocated to photosynthetic leaf tissue. We expected that this response would be driven by a reduction in the cost of acquiring N, which would cause trees to sacrifice efficient N use to enable more efficient use of other limiting resources (i.e., water). We hypothesized similar leaf responses to increasing soil pH.

## 3.2 Methods

### 3.2.1 *Study site description*

We conducted this study in summer 2019 at three stands located within a 20-km radius of Ithaca, NY, USA (42.444 °N, 76.502 °W). All stands contain mature, closed-canopy forests dominated by deciduous tree species. Stands contained abundant sugar maple (*Acer saccharum* Marshall), American beech (*Fagus grandifolia* Ehrh.), and white ash (*Fraxinus americana* L.), accounting for 43%, 15%, and 17% of the total aboveground biomass across the three stands, respectively, with less frequent red maple (*Acer rubrum* L.; 9% of total aboveground biomass) and red oak occurrences (*Quercus rubra* L.; 10% of total aboveground biomass). Soils at each site were broadly classified as a channery silt loam Inceptisols using the USDA NRCS Web Soil Survey data product (Soil Survey Staff 2022). Between 2006 and 2020, study sites averaged 972 mm of precipitation per year and had an average temperature of 7.9 °C per a weather station located near the Cornell University campus (42.449 °N, 76.449 °W) part of the NOAA NCEI Global Historical Climatology Network (Menne et al. 2012).

520 3.2.2 *Experimental design*

521 Four 40 m x 40 m plots were set up at each site in 2009, each with an  
522 additional 10 m buffer along plot perimeters (60 m x 60 m total). The plots  
523 were set up as a nitrogen-by-pH field manipulation experiment, with one each of  
524 four treatments at each site. Two nitrogen treatments were applied, both at 50  
525 kg N ha<sup>-1</sup> yr<sup>-1</sup>, as either sodium nitrate (NaNO<sub>3</sub>) to raise soil pH, or ammonium  
526 sulfate ((NH<sub>4</sub>)<sub>2</sub>SO<sub>4</sub>) to acidify; an elemental sulfur treatment was selected to acid-  
527 ify without N, applied at the same rate of S addition (57 kg S ha<sup>-1</sup> yr<sup>-1</sup>); and  
528 control plots received no additions. All amendments were added in pelletized form  
529 using hand-held fertilizer spreaders to both the main plots and buffers. Amend-  
530 ments were divided into three equal doses distributed across the growing season  
531 from 2011-2017 and added as a single dose from 2018 onward. During 2019, plots  
532 were fertilized during the week of May 20.

533 3.2.3 *Leaf gas exchange and trait measurements*

534 We sampled one leaf each from 6 to 10 individuals per plot between June  
535 25 and July 12, 2019 for gas exchange measurements (Table S1). Leaves were  
536 collected from deciduous broadleaf trees represented across all sites and plots and  
537 were replicated in efforts to mimic the species abundance of each plot at each  
538 site. We also attempted to collect leaves from the upper canopy to reduce differ-  
539 ential shading effects on leaf physiology. Leaves were accessed by pulling down  
540 small branches using an arborist's slingshot and weighted beanbag attached to a  
541 throwline. Branches were immediately recut under deionized water and remained  
542 submerged to reduce stomatal closure and avoid xylem embolism (as in Smith &

543 Dukes, 2018) until gas exchange data were collected.

544 Randomly selected leaves with little to no visible external damage were  
 545 attached to a Li-COR LI-6800 (Li-COR Bioscience, Lincoln, Nebraska, USA)  
 546 portable photosynthesis machine to measure net photosynthesis ( $A_{\text{net}}$ ;  $\mu\text{mol m}^{-2} \text{s}^{-1}$ ),  
 547 stomatal conductance ( $g_{\text{sw}}$ ;  $\text{mol m}^{-2} \text{s}^{-1}$ ), and intercellular  $\text{CO}_2$  concentration  
 548 ( $C_i$ ;  $\mu\text{mol mol}^{-1}$ ) at different reference  $\text{CO}_2$  concentrations ( $C_a$ ;  $\mu\text{mol mol}^{-1}$ )  
 549 concentrations (i.e., an  $A_{\text{net}}/C_i$  curve) under saturating light conditions (2,000  
 550  $\mu\text{mol m}^{-2} \text{s}^{-1}$ ). Reference  $\text{CO}_2$  concentrations followed the sequence: 400, 300,  
 551 200, 100, 50, 400, 400, 600, 800, 1000, 1200, 1500, and 2000  $\mu\text{mol mol}^{-1} \text{CO}_2$ . Leaf  
 552 temperatures were not controlled in the cuvette and ranged from 21.8 °C to 31.7  
 553 °C (mean $\pm$ SD:  $27.2 \pm 2.2$  °C). A linear and second order log-polynomial nonlinear  
 554 regression suggested no effect of temperature on stomatal conductance measured  
 555 at 400  $\mu\text{mol mol}^{-1} \text{CO}_2$  or net photosynthesis measured at  $\mu\text{mol mol}^{-1} \text{CO}_2$  (Ta-  
 556 ble S2-3; Fig. S1). All  $A_{\text{net}}/C_i$  curves were generated within one hour of branch  
 557 severance.

558 Leaf morphological and chemical traits were collected on the same leaf used  
 559 to generate each  $A_{\text{net}}/C_i$  curve. Images of each leaf were taken using a flat-bed  
 560 scanner to determine fresh leaf area using the ‘LeafArea’ R package (Katabuchi  
 561 2015), which automates leaf area calculations using ImageJ software (Schneider  
 562 et al. 2012). Each leaf was dried at 65°C for at least 48 hours, weighed, and  
 563 ground using a Retsch MM200 ball mill grinder (Verder Scientific, Inc., Newtown,  
 564 PA, USA) until homogenized. Leaf mass per area ( $M_{\text{area}}$ ,  $\text{g m}^{-2}$ ) was calculated  
 565 as the ratio of dry leaf biomass to fresh leaf area. Using a subsample of ground and  
 566 homogenized leaf biomass, leaf N content ( $N_{\text{mass}}$ ;  $\text{gN g}^{-1}$ ) and leaf  $\delta^{13}\text{C}$  (‰, rela-

567 tive to VPDB) were measured at the Cornell Stable Isotope Lab with an elemental  
 568 analyzer (NC 2500, CE Instruments, Wigan, UK) interfaced to an isotope ratio  
 569 mass spectrometer (Delta V Isotope Ratio Mass Spectrometer, ThermoFisher Sci-  
 570 entific, Waltham, MA, USA). Leaf N content per unit leaf area ( $N_{\text{area}}$ ; gN m<sup>-2</sup>)  
 571 was calculated by multiplying  $N_{\text{mass}}$  by  $M_{\text{area}}$ .

572 We used leaf  $\delta^{13}\text{C}$  values to estimate  $\chi$  (unitless), which is an isotope-  
 573 derived estimate of the leaf  $C_i:C_a$  ratio. While intercellular and atmospheric CO<sub>2</sub>  
 574 concentrations were directly measured during each  $A_{\text{net}}/C_i$  curve, deriving  $\chi$  from  
 575  $\delta^{13}\text{C}$  provides a more integrative estimate of the  $C_i:C_a$  over an individual leaf's  
 576 lifespan. We derived  $\chi$  following the approach of Farquhar et al. (1989) decribed  
 577 in Cernusak et al. (2013):

$$\chi = \frac{\Delta^{13}\text{C} - a}{b - a} \quad (3.1)$$

578 where  $\Delta^{13}\text{C}$  represents the relative difference between leaf  $\delta^{13}\text{C}$  (‰) and air  $\delta^{13}\text{C}$   
 579 (‰), and is calculated from the following equation:

$$\Delta^{13}\text{C} = \frac{\delta^{13}\text{C}_{\text{air}} - \delta^{13}\text{C}_{\text{leaf}}}{1 + \delta^{13}\text{C}_{\text{leaf}}} \quad (3.2)$$

580 where  $\delta^{13}\text{C}_{\text{air}}$  is assumed to be -8‰ (Keeling et al. 1979; Farquhar et al. 1989), a  
 581 represents the fractionation between <sup>12</sup>C and <sup>13</sup>C due to diffusion in air, assumed  
 582 to be 4.4‰, and b represents the fractionation caused by Rubisco carboxylation,  
 583 assumed to be 27‰ (Farquhar et al. 1989).

### 584 3.2.4 $A_{\text{net}}/C_i$ curve-fitting and parameter estimation

585 We fit  $A_{\text{net}}/C_i$  curves of each individual using the ‘fitaci’ function in the  
 586 ‘plantecophys’ R package (Duursma 2015). This function estimates the maximum  
 587 rate of Rubisco carboxylation  $V_{\text{cmax}}$ ;  $\mu\text{mol m}^{-2} \text{s}^{-1}$ ) and maximum rate of electron  
 588 transport for RuBP regeneration ( $J_{\text{max}}$ ;  $\mu\text{mol m}^{-2} \text{s}^{-1}$ ) based on the Farquhar,  
 589 von Caemmerer, and Berry biochemical model of  $C_3$  photosynthesis (Farquhar  
 590 et al. 1980). For each curve fit, we included triose phosphate utilization (TPU)  
 591 limitation to avoid underestimating  $J_{\text{max}}$  (Gregory et al. 2021). Curves were  
 592 visually examined to confirm the likely presence of TPU limitation.

593 We determined Michaelis-Menten coefficients for Rubisco affinity to  $\text{CO}_2$   
 594 ( $K_c$ ;  $\mu\text{mol mol}^{-1}$ ) and  $\text{O}_2$  ( $K_o$ ;  $\mu\text{mol mol}^{-1}$ ), and the  $\text{CO}_2$  compensation point  
 595 ( $\Gamma^*$ ;  $\mu\text{mol mol}^{-1}$ ) using leaf temperature and equations described in Medlyn et al.  
 596 (2002) and derived in Bernacchi et al. (2001). Specifically,  $K_c$  and  $K_o$  were  
 597 calculated as:

$$K_c = 404.9 * \exp^{\frac{79430(T_k - 298)}{298RT_k}} \quad (3.3)$$

598 and

$$K_o = 278.4 * \exp^{\frac{36380(T_k - 298)}{298RT_k}} \quad (3.4)$$

599 while  $\Gamma^*$  was calculated as:

$$\Gamma^* = 42.75 * \exp^{\frac{37830(T_k - 298)}{298RT_k}} \quad (3.5)$$

600 In all three equations,  $T_k$  is the leaf temperature (in Kelvin) during each  $A_{\text{net}}/C_i$   
 601 curve and  $R$  is the universal gas constant ( $8.314 \text{ J mol}^{-1} \text{ K}^{-1}$ ).

602 We standardized  $V_{\text{cmax}}$  and  $J_{\text{max}}$  estimates to  $25^\circ\text{C}$  using a modified Ar-  
 603 rhenius equation (Kattge and Knorr 2007):

$$k_{25} = \frac{k_{\text{obs}}}{e^{\frac{H_a(T_{\text{obs}} - T_{\text{ref}})}{T_{\text{ref}}RT_{\text{obs}}}} * \frac{1 + e^{\frac{T_{\text{ref}}\Delta S - H_d}{T_{\text{ref}}}}}{1 + e^{\frac{T_{\text{obs}}\Delta S - H_d}{T_{\text{obs}}}}}} \quad (3.6)$$

604  $k_{25}$  represents the standardized  $V_{\text{cmax}}$  or  $J_{\text{max}}$  rate at  $25^\circ\text{C}$ ,  $k_{\text{obs}}$  represents  
 605 the  $V_{\text{cmax}}$  or  $J_{\text{max}}$  estimate at the average leaf temperature measured inside the  
 606 cuvette during the  $A_{\text{net}}/C_i$  curve.  $H_a$  is the activation energy of  $V_{\text{cmax}}$  ( $71,513$   
 607  $\text{J mol}^{-1}$ ) Kattge and Knorr (2007) or  $J_{\text{max}}$  ( $49,884 \text{ J mol}^{-1}$ ) (Kattge and Knorr  
 608 2007).  $H_d$  represents the deactivation energy of both  $V_{\text{cmax}}$  and  $J_{\text{max}}$  ( $200,000 \text{ J}$   
 609  $\text{mol}^{-1}$ ) (Medlyn et al. 2002), and  $R$  represents the universal gas constant ( $8.314$   
 610  $\text{J mol}^{-1} \text{ K}^{-1}$ ).  $T_{\text{ref}}$  represents the standardized temperature of  $298.15 \text{ K}$  ( $25^\circ\text{C}$ )  
 611 and  $T_{\text{obs}}$  represents the mean leaf temperature (in  $\text{K}$ ) during each  $A_{\text{net}}/C_i$  curve.  
 612  $\Delta S$  is an entropy term that (Kattge and Knorr 2007) derived as a linear relation-  
 613 ship with average growing season temperature ( $T_g$ ;  $^\circ\text{C}$ ), where:

$$\Delta S_{vcmax} = -1.07 T_g + 668.39 \quad (3.7)$$

614 and

$$\Delta S_{jmax} = -0.75 T_g + 659.70 \quad (3.8)$$

We estimated  $T_g$  in Equations 3.7 and 3.8 based on mean daily (24-hour) air temperature of the 30 days leading up to the day of each sample collection using the same weather station reported in the site description. We then used  $V_{\text{cmax25}}$  and  $J_{\text{max25}}$  estimates to calculate the ratio of  $J_{\text{max25}}$  to  $V_{\text{cmax25}}$  ( $J_{\text{max25}}:V_{\text{cmax25}}$ ; unitless).

### 3.2.5 *Proportion of leaf nitrogen allocated to photosynthesis and structure*

We used equations from Niinemets and Tenhunen (1997) to estimate the proportion of leaf N content allocated to Rubisco and bioenergetics. The proportion of leaf N allocated to Rubisco ( $\rho_{\text{rub}}$ ; gN gN<sup>-1</sup>) was calculated as a function of  $V_{\text{cmax25}}$  and  $N_{\text{area}}$ :

$$\rho_{\text{rubisco}} = \frac{V_{\text{cmax25}} N_r}{V_{\text{cr}} N_{\text{area}}} \quad (3.9)$$

where  $N_r$  is the amount of nitrogen in Rubisco, set to 0.16 gN (gN in Rubisco)<sup>-1</sup> and  $V_{\text{cr}}$  is the maximum rate of RuBP carboxylation per unit Rubisco protein, set to 20.5  $\mu\text{mol CO}_2$  (g Rubisco)<sup>-1</sup>. The proportion of leaf nitrogen allocated to bioenergetics ( $\rho_{\text{bioe}}$ ; gN gN<sup>-1</sup>) was similarly calculated as a function of  $J_{\text{max25}}$  and  $N_{\text{area}}$ :

$$\rho_{\text{bioe}} = \frac{J_{\text{max25}} N_b}{J_{\text{mc}} N_{\text{area}}} \quad (3.10)$$

where  $N_b$  is the amount of nitrogen in cytochrome f, set to 0.12407 gN ( $\mu\text{mol cytochrome f}$ )<sup>-1</sup> assuming a constant 1: 1: 1.2 cytochrome f: ferredoxin NADP reductase: coupling factor molar ratio (Evans and Seemann 1989; Niinemets and



633 Tenhunen 1997), and  $J_{mc}$  is the capacity of electron transport per cytochrome f,  
 634 set to  $156 \mu\text{mol electron } (\mu\text{mol cytochrome f})^{-1}\text{s}^{-1}$ .

635 We estimated the proportion of leaf N content allocated to photosynthetic  
 636 tissue ( $\rho_{\text{photo}}$ ;  $\text{gN gN}^{-1}$ ) as the sum of  $\rho_{\text{rub}}$  and  $\rho_{\text{bioe}}$ . This calculation is an un-  
 637 derestimate of the proportion of leaf N allocated to photosynthetic tissue because  
 638 it does not include N allocated to light harvesting proteins. This leaf N pool was  
 639 not included because we did not perform chlorophyll extractions on focal leaves.  
 640 However, the proportion of leaf N content allocated to light harvesting proteins  
 641 tends to be small relative to  $\rho_{\text{rub}}$  and  $\rho_{\text{bioe}}$ , and may scale with changes in  $\rho_{\text{rub}}$   
 642 and  $\rho_{\text{bioe}}$  (Ninemets and Tenhunen 1997).

643 Finally, we estimated the proportion of leaf N content allocated to struc-  
 644 tural tissue ( $\rho_{\text{str}}$ ;  $\text{gN gN}^{-1}$ ) using an empirical equation from Onoda et al. (2017):

$$N_{cw} = 0.000355 * M_{area}^{1.39} \quad (3.11)$$

645 where  $N_{cw}$  is the leaf N content allocated to cell walls ( $\text{gN m}^{-2}$ ).  $\rho_{\text{str}}$  was estimated  
 646 by dividing  $N_{cw}$  by  $N_{\text{area}}$ .

### 647 3.2.6 Tradeoffs between nitrogen and water use

648 Photosynthetic nitrogen use efficiency (PNUE;  $\mu\text{mol CO}_2 \text{ mol}^{-1} \text{ N s}^{-1}$ )  
 649 was calculated by dividing  $A_{\text{net}}$  by  $N_{\text{area}}$ , first converting  $N_{\text{area}}$  to  $\text{mol N m}^{-2}$   
 650 using the molar mass of N ( $14 \text{ g mol}^{-1}$ ). We used  $\chi$  as an indicator of water  
 651 use efficiency, which exploratory analyses suggest had similar responses to soil N  
 652 availability and pH as intrinsic water use efficiency measured from gas exchange

( $A_{\text{net}}/g_s$ ). Tradeoffs between nitrogen and water use were determined by calculating the ratio of  $N_{\text{area}}$  to  $\chi$  ( $N_{\text{area}}:\chi$ ; g N m<sup>-2</sup>) and  $V_{\text{cmax25}}$  to  $\chi$  ( $V_{\text{cmax25}}:\chi$ ;  $\mu\text{mol m}^{-2} \text{ s}^{-1}$ ). This approach is similar to tradeoff calculations in which nitrogen-water use tradeoffs are measured as the ratio of  $N_{\text{area}}$  or  $V_{\text{cmax25}}$  to  $g_s$  (Paillassa et al. 2020; Bialic-Murphy et al. 2021). In this study, we quantify these relationships using  $\chi$  in lieu of  $g_s$  because  $g_s$  rapidly changes with environmental conditions and therefore may have been altered by recent tree branch severance and/or placement in the cuvette.

### 3.2.7 *Soil nitrogen availability and pH*

To characterize soil N availability at the time of our leaf gas exchange measurements, we used mixed bed resin bags to quantify mobile ammonium-N and nitrate-N concentrations in each plot. Lycra mesh bags were filled with 5 g of Dowex® Marathon MR-3 hydrogen and hydroxide form resin (MilliporeSigma, Burlington, MA USA) and sealed with a zip tie. Each bag was activated by soaking in 0.5 M HCl for 20 minutes, then in 2 M NaCl until pH of the saline solution stabilized, as described in Allison et al. (2008). Five resin bags were inserted about 10 cm below the soil surface at each plot on June 25, 2019: one near each of the four plot corners and one near the plot center. All resin bags were collected 24 days later on July 19, 2019 and were frozen until extracted.

Prior to anion and cation extraction, each resin bag was rinsed with ultrapure water (MilliQ IQ 7000; Millipore Sigma, Burlington, MA) to remove any surface soil residues. Anions and cations were extracted from surface-cleaned resin bags by individually soaking and shaking each bag in 100 mL of a 0.1 M HCl/2.0

676 M NaCl matrix for one hour. Using a microplate reader (Biotek Synergy H1;  
 677 Biotek Instruments, Winooski, VT USA), nitrate-N concentrations were quanti-  
 678 fied spectrophotometrically at 540 nm with the end product of a single reagent  
 679 vanadium (III) chloride reaction (Doane and Horwáth 2003), and ammonium-N  
 680 concentrations quantified at 650 nm with the end product of a modified phenol-  
 681 hypochlorite reaction (Weatherburn 1967; Rhine et al. 1998). Both the single  
 682 reagent vanadium (III) chloride and modified phenol-hypochlorite methodologies  
 683 have been well established for determining nitrate-N and ammonium-N concen-  
 684 trations in resin bag extracts (Arnone 1997; Allison et al. 2008). We used a  
 685 series of negative and positive controls throughout each well plate to verify the  
 686 accuracy and precision of our measurements, assaying each resin bag extract and  
 687 control in triplicate. Soil N availability was estimated as the sum of the nitrate-N  
 688 and ammonium-N concentration in each resin bag, normalized per g of resin and  
 689 duration in the field ( $\mu\text{g N g}^{-1} \text{ resin d}^{-1}$ ), then subsequently averaged across all  
 690 resin bags in a plot for a plot-level mean.

691        Soil pH was measured on 0-10 cm mineral soil samples collected prior to  
 692 fertilization in 2019. Near each of the four plot corners, three 5.5 cm diameter soil  
 693 cores were collected after first removing the forest floor where present. Each set  
 694 of three cores was placed in a plastic bag, and later composited by hand mixing  
 695 and sieved to 4mm. Soil pH was determined for a 1:2 soil:water slurry (10 g field-  
 696 moist soil to 20 mL DI water) of each sample using an Accumet AB15 pH meter  
 697 with flushable junction probe (Fisher Scientific; Hampton, NH, USA), and was  
 698 estimated at the plot level as the mean soil pH within each plot.

### 699 3.2.8 *Statistical analyses*

700 We built two separate series of linear mixed-effects models to explore effects  
 701 of soil N availability, soil pH, species, and leaf N content on leaf physiological  
 702 traits. In the first series of linear mixed-effects models, we explored the effect  
 703 of soil N availability, soil pH, and species on leaf N content, leaf photosynthesis,  
 704 stomatal conductance, and nitrogen-water use tradeoffs. Models included plot-  
 705 level soil N availability and plot-level soil pH as continuous fixed effects, species  
 706 as a categorical fixed effect, and site as a categorical random intercept term.  
 707 Interaction terms between fixed effects were not included due to the small number  
 708 of experimental plots. We built a series of separate models with this independent  
 709 variable structure to quantify individual effects of soil N availability, soil pH,  
 710 and species on  $N_{\text{area}}$ ,  $M_{\text{area}}$ ,  $N_{\text{mass}}$ ,  $A_{\text{net}}$ ,  $V_{\text{cmax25}}$ ,  $J_{\text{max25}}$ ,  $J_{\text{max25}}:V_{\text{cmax25}}$ ,  $\rho_{\text{rubisco}}$ ,  
 711  $\rho_{\text{bioenergetics}}$ ,  $\rho_{\text{photo}}$ ,  $\rho_{\text{structure}}$ ,  $\chi$ , PNUE,  $N_{\text{area}}:\chi$ , and  $V_{\text{cmax25}}:\chi$ .

712 A second series of linear mixed-effects models were built to investigate  
 713 relationships between leaf N content and photosynthetic parameters. Statistical  
 714 models included  $N_{\text{area}}$  as a single continuous fixed effect with species and site des-  
 715 ignated as individual random intercept terms. We used this independent variable  
 716 structure to quantify individual effects of leaf N content on  $A_{\text{net}}$ ,  $V_{\text{cmax25}}$ ,  $J_{\text{max25}}$ ,  
 717  $J_{\text{max25}}:V_{\text{cmax25}}$ , and  $\chi$ .

718 For all linear mixed-effects models, we used Shapiro-Wilk tests of normal-  
 719 ity to determine whether linear mixed-effects models satisfied residual normality  
 720 assumptions. If residual normality assumptions were not met, then models were  
 721 fit using dependent variables that were natural log transformed. If residual nor-  
 722 mality assumptions were still not met (Shapiro-Wilk:  $p < 0.05$ ), then models were

723 fit using dependent variables that were square root transformed. All residual nor-  
 724 mality assumptions for both sets of models that did not originally satisfy residual  
 725 normality assumptions were met with either a natural log or square root data  
 726 transformation (Shapiro-Wilk:  $p > 0.05$  in all cases).

727 In the first series of models, models for  $N_{\text{area}}$ ,  $M_{\text{area}}$ ,  $N_{\text{mass}}$ ,  $V_{\text{cmax25}}$ ,  $J_{\text{max25}}$ ,  
 728  $\chi$ ,  $N_{\text{area}}:\chi$ , and  $V_{\text{cmax25}}:\chi$ ,  $\rho_{\text{rubisco}}$ ,  $\rho_{\text{bioenergetics}}$ ,  $\rho_{\text{photo}}$ ,  $\rho_{\text{structure}}$  satisfied residual  
 729 normality assumptions without data transformations (Shapiro-Wilk:  $p > 0.05$  in  
 730 all cases). The model for  $J_{\text{max25}}:V_{\text{cmax25}}$  satisfied residual normality assumptions  
 731 with a natural log data transformation, while models for  $A_{\text{net}}$  and PNUE each  
 732 satisfied residual normality assumptions with square root data transformations.  
 733 In the second series of models, models for  $V_{\text{cmax25}}$ ,  $J_{\text{max25}}$ ,  $\chi$ , and  $V_{\text{cmax25}}:\chi$  satisfied  
 734 residual normality assumptions without data transformations (Shapiro-Wilk:  $p$   
 735  $> 0.05$  in all cases). The model for  $J_{\text{max25}}:V_{\text{cmax25}}$  required a natural log data  
 736 transformation and the model for  $A_{\text{net}}$  required a square root data transformation  
 737 (Shapiro-Wilk:  $p > 0.05$  in both cases).

738 In all models, we used the ‘lmer’ function in the ‘lme4’ R package (Bates  
 739 et al. 2015) to fit each model and the ‘Anova’ function in the ‘car’ R package (Fox  
 740 and Weisberg 2019) to calculate Type II Wald’s  $\chi^2$  and determine the significance  
 741 level ( $\alpha = 0.05$ ) of each fixed effect coefficient. Finally, we used the ‘emmeans’  
 742 R package (Lenth, 2019) to conduct post-hoc comparisons using Tukey’s tests,  
 743 where degrees of freedom were approximated using the Kenward-Roger approach  
 744 (Kenward and Roger 1997). All analyses and plots were conducted in R version  
 745 4.1.1 (R Core Team 2021)). All figure regression lines and associated 95% confi-  
 746 dence interval error bars were plotted using predictions generated across the soil

747 nitrogen availability gradient using the ‘emmeans’ R package (Lenth 2019).

### 748 3.3 Results

#### 749 3.3.1 *Leaf N content*

750       Increasing soil N availability generally increased  $N_{\text{area}}$  (Table 3.1; Fig.  
751 3.1a). This pattern was driven by an increase in  $N_{\text{mass}}$  (Table 3.1; Fig. 3.1c)  
752 and a marginal increase in  $M_{\text{area}}$  (Table 1; Fig. 1e) with increasing soil N avail-  
753 ability. There was no effect of soil pH on  $N_{\text{area}}$ ,  $N_{\text{mass}}$ , or  $M_{\text{area}}$  (Table 1); however,  
754 we did observe strong differences in  $N_{\text{area}}$  (Fig. 1b),  $N_{\text{mass}}$  (Fig. 1d), and  $M_{\text{area}}$   
755 (Fig. 1e) between species (Table 1).

**756** [placeholder for Table 1]

**757**

[placeholder for Fig 1]



**758** 3.3.2 *Net photosynthesis and leaf biochemistry*

**759** Increasing soil N availability generally had no effect on  $A_{\text{net}}$ ,  $V_{\text{cmax25}}$ ,  $J_{\text{max25}}$ ,  
**760** or  $J_{\text{max25}}:V_{\text{cmax25}}$  (Figs. 2a, 2d, 2g). We also observed strong species effects on all  
**761** measured leaf photosynthetic traits (Table 2; Figs. 2b, 2e, 2h). Increasing soil  
**762** pH had a marginal negative effect on  $A_{\text{net}}$ , but had no effect on  $V_{\text{cmax25}}$ ,  $J_{\text{max25}}$ ,  
**763** or  $J_{\text{max25}}:V_{\text{cmax25}}$  (Table 2). There was a weak positive effect of increasing  $N_{\text{area}}$  on  
**764**  $A_{\text{net}}$  (Fig. 2c), but quite strong positive effects of increasing  $N_{\text{area}}$  on  $V_{\text{cmax25}}$  and  
**765**  $J_{\text{max25}}$  (Table 2; Fig. 2f and 2i).

**766** [placeholder for Table 2]

**767**

[placeholder for Fig 2]

**768** 3.3.3 *Leaf N allocation*

**769**        Neither soil N availability nor soil pH affected the proportion of leaf N  
**770** allocated to Rubisco or bioenergetics (Table 3; Fig. 3a, Fig. 3c), nor was there  
**771** any subsequent effect on the proportion of leaf N allocated to photosynthesis  
**772** (Table 3; Fig. 3f). We also found no effect of soil N availability or soil pH on the  
**773** proportion of leaf N allocated to structure (Table 3; Fig 3g). Species varied in  
**774** the proportion of leaf N allocated to Rubisco, photosynthesis, and structure (Fig  
**775** 3b, Fig. 3d, Fig 3h), with no detectable species effect on the proportion of leaf N  
**776** allocated to bioenergetics (Table 3).

**777** [placeholder for Table 3]

**778** [placeholder for Fig 3]

### 779 3.3.4 *Tradeoffs between nitrogen and water use*

780           Although soil N availability did not affect  $\chi$  (Table 4; Fig. 4a), increasing  
781 soil N availability decreased PNUE (Table 4; Fig. 4d) and increased the ratio of  
782  $N_{\text{area}}:\chi$  (Table 4; Fig. 4f). Specifically, this response yielded a 26% reduction in  
783 PNUE and 37% stimulation in  $N_{\text{area}}:\chi$  across the soil nitrogen availability gradient.  
784 There was no apparent effect of soil N availability on  $V_{\text{cmax25}}:\chi$  (Table 4; Fig. 4h).  
785 Increasing soil pH had a weak marginal negative effect on PNUE, but did not  
786 influence  $\chi$ ,  $N_{\text{area}}:\chi$ , or  $V_{\text{cmax25}}:\chi$  (Table 4). We also observed differences in  $\chi$   
787 (Fig. 4b), PNUE (Fig. 4e),  $N_{\text{area}}:\chi$  (Fig. 4g), and  $V_{\text{cmax25}}:\chi$  (Fig. 4i) between  
788 species (Table 4). Finally, increasing  $N_{\text{area}}$  had a strong negative effect on  $\chi$  (Table  
789 4; Fig. 4c) and a strong positive effect on  $V_{\text{cmax25}}:\chi$  (Table 4; Fig. 4j).

**790** [placeholder for Table 4]



**791** [placeholder for Fig 4]

## 792 3.4 Discussion

793       Photosynthetic least-cost theory provides an explanation for understand-  
 794 ing relationships between soil nutrient availability, leaf nutrient allocation, and  
 795 photosynthetic capacity. The theory suggests that plants acclimate to a given  
 796 environment by optimizing leaf photosynthesis rates at the lowest summed cost  
 797 of using nutrients and water Prentice et al. (2014), Wang et al. (2017), Smith  
 798 et al. (2019), Paillassa et al. (2020). The theory predicts that an increase in  
 799 soil nutrient availability should allow similar photosynthesis rates to be achieved  
 800 with increased leaf nutrient content and photosynthetic capacity (i.e.,  $V_{\text{cmax}25}$  and  
 801  $J_{\text{max}25}$ ) at lower leaf  $C_i:C_a$  ( $\chi$ ), resulting in an increase in water use efficiency,  
 802 decrease in nutrient use efficiency, and increase in both leaf nutrient content and  
 803 photosynthetic capacity per unit  $\chi$ . The theory predicts similar leaf responses to  
 804 increasing soil pH under acidic conditions, presumably due to generally faster nu-  
 805 trient cycle dynamics and consequent reductions in the cost of acquiring nutrients  
 806 relative to water with increasing soil pH (Wang et al. 2017; Paillassa et al. 2020;  
 807 Dong et al. 2020).

808       Supporting the theory, we showed that increasing soil N availability was  
 809 associated with increased leaf N content (Fig 3.1a, 3.1c), a pattern that reduced  
 810 photosynthetic N use efficiency (Fig 3.4d) and increased leaf N content per unit  
 811  $\chi$  (Fig 3.4f). Increasing soil N coincided with slight, but non-significant decreases  
 812 in  $\chi$  and increases in  $V_{\text{cmax}25}$  and  $J_{\text{max}25}$  ( $p < 0.2$ ). The positive trend between  
 813 soil N availability and photosynthetic capacity was supported by the concurrent  
 814 strong increase in leaf N content with increasing soil N availability, which resulted  
 815 in no change in the proportion of leaf N content allocated to photosynthesis across

the soil N availability gradient. Additionally, leaf N content exhibited a strong negative correlation with  $\chi$ , indicative of strong nitrogen-water use tradeoffs at the leaf level. Responses tended to vary more due to soil N availability than soil pH. Overall, these findings are consistent with the nutrient-water use tradeoffs predicted from theory.

### 3.4.1 *Soil nitrogen availability modifies tradeoffs between nitrogen and water use*

In support of expected least-cost outcomes and past environmental gradient studies (Dong et al. 2017; Paillassa et al. 2020), we found that increasing soil N availability was associated with increased leaf N content. Soil N availability had smaller impacts on measures of net photosynthesis and  $\chi$ , which led to reductions in PNUE and increases in leaf N content per unit  $\chi$ , as expected from theory. Photosynthetic least-cost theory suggests that reductions in PNUE should be driven by an increase in the proportion of leaf N allocated to photosynthetic tissue, a pattern that should allow plants to achieve optimal photosynthetic rates with greater photosynthetic capacity to make better use of available light. Contrasting theory predictions, we found no effect of soil N availability on photosynthetic capacity. However, photosynthetic capacity did tend to increase with increasing soil N availability ( $p < 0.20$ ; Table 2) resulting in no effect of soil N availability on the relative fraction of leaf N allocated to photosynthesis, Rubisco, or bioenergetics (Fig. 3). These lines of evidence support the idea that trees use additional N to support increased leaf N allocation toward photosynthetic tissue and enhance photosynthetic capacity (Wright et al. 2003).

Soil N availability had a stronger effect on leaf N than photosynthetic ca-

839 capacity. This pattern suggests that additional plant N uptake due to increased  
 840 soil N availability was also being used to support non-photosynthetic N pools,  
 841 possibly to structural tissue or stress-induced amino acid and polyamine synthe-  
 842 sis (Minocha et al. 2000; Onoda et al. 2004; Bubier et al. 2011). While we  
 843 found no change in the proportion of leaf N allocated to leaf structural tissue, the  
 844 overall stimulation in leaf N content with increasing soil N availability suggests an  
 845 increase in the net amount of N invested in leaf structural tissue along the N avail-  
 846 ability gradient. Importantly, leaf N allocated to structure was calculated using  
 847 an empirical relationship between  $M_{\text{area}}$  and the amount of leaf N allocated to cell  
 848 walls (Onoda et al. 2017). As the generality of relationships between  $M_{\text{area}}$  and  
 849 the amount of leaf N allocated to cell walls has been called into question (Harrison  
 850 et al. 2009), future work should consider explicitly measuring N allocation to cell  
 851 wall tissue and stress-induced amino acid synthesis to confirm these patterns.

852         In opposition to patterns expected from least cost theory, increasing soil  
 853 N availability had no apparent effect on  $\chi$  (Fig. 4a). Interestingly, despite the  
 854 null effect of soil N availability on  $\chi$ , we observed a strong negative effect of  
 855 increasing  $N_{\text{area}}$  on  $\chi$  (Fig. 4c), consistent with the nitrogen-water use tradeoffs  
 856 expected from theory. The null response of  $\chi$  to increasing soil N availability may  
 857 have been due to a lack of water limitation in the system, given that the area  
 858 received approximately 20% more precipitation (1167 mm) during the 12-month  
 859 period leading up to our measurement period than normally expected (972 mm).  
 860 However, droughts can and do occur in temperate forests of the northeastern  
 861 United States (Sweet et al. 2017), so the observed increase in leaf N content  
 862 with increasing soil N availability could be a strategy that allows trees to hedge

863 bets against drier than normal growing seasons (Onoda et al. 2004; Onoda et al.  
864 2017; Hallik et al. 2009). As was suggested in Paillassa et al. (2020), and more  
865 recently by Querejeta et al. (2022), negative effects of soil N availability on  $\chi$  may  
866 increase with increasing aridity. This strategy would be especially advantageous if  
867 it allows individuals growing in arid regions to maintain carbon assimilation rates  
868 with reduced water loss. Future work should attempt to quantify interactive roles  
869 of climate and soil nitrogen availability on nitrogen-water use tradeoffs, which  
870 could be done by leveraging coordinated and multi-factor nutrient (Borer et al.  
871 2014) and water (Knapp et al. 2017) manipulation experiments across broad  
872 climatic gradients.

#### 873 3.4.2 *Soil pH did not modify tradeoffs between nitrogen and water usage*

874 While the primary purpose of this study was to examine the role of soil N  
875 availability on nitrogen-water use tradeoffs, our experimental design manipulated  
876 both soil N and pH, providing an opportunity to isolate the roles of these variables.  
877 Previous correlational studies along environmental gradients identified soil pH as  
878 a particularly important factor that can modify tradeoffs between nutrient and  
879 water use (Smith et al. 2019; Paillassa et al. 2020; Westerland et al. 2023)  
880 and the proportion of leaf nitrogen allocated to photosynthesis (Luo et al. 2021).  
881 Such studies implied that these patterns may be driven by reductions in the cost of  
882 acquiring nutrients relative to water with increasing pH, which may be exacerbated  
883 in acidic soils.

884 Consistent with theory (Wright et al. 2003; Prentice et al. 2014), our  
885 results indicate that increasing soil pH was negatively associated with PNUE.

886 However, there was no effect of soil pH on leaf N content,  $\chi$ , or leaf N content per  
 887 unit  $\chi$ , most likely because the experimental N additions increased soil N sup-  
 888 ply while both increasing (sodium nitrate) and decreasing (ammonium sulfate)  
 889 soil pH. These results suggest that soil pH did not play a major role in modify-  
 890 ing expected photosynthetic least-cost theory patterns, contrasting findings from  
 891 Paillassa et al. (2020) and other gradient studies that note positive effects of in-  
 892 creasing soil pH on leaf N content, Rubisco carboxylation, and  $\chi$  (Viet et al. 2013;  
 893 Cornwell et al. 2018; Luo et al. 2021). Instead, null responses to soil pH show  
 894 that leaf photosynthetic parameters depend more on soil N availability than pH  
 895 per se, and that inferences from gradient studies might be confounding covariation  
 896 between N availability and soil acidity.

### 897 3.4.3 *Species identity explains a large amount of variation in leaf and whole* 898 *plant traits*

899 Species generally explained a larger amount of variation in measured leaf  
 900 traits than soil N availability or soil pH. Interspecies variation is an important  
 901 factor to consider when deducing mechanisms that drive photosynthetic least-  
 902 cost theory, particularly for species that form distinct mycorrhizal associations or  
 903 have different photosynthetic pathways, growth forms, or leaf habit (Espelta et al.  
 904 2005; Adams et al. 2016; Bialic-Murphy et al. 2021; Scott and Smith 2022). The  
 905 need to consider species may also be important when comparing nutrient-water  
 906 use tradeoffs in early and late successional species, or in species with different  
 907 resource economic strategies (Abrams and Mostoller 1995; Ellsworth and Reich  
 908 1996; Wright et al. 2004; Reich 2014; Onoda et al. 2017; Ziegler et al. 2020).

909           A strength of the study design and sampling effort is that it controls for  
 910 many species differences that should modify nitrogen-water use tradeoffs expected  
 911 from theory. All tree species measured in this study shared the leaf habit of decid-  
 912 uous broadleaves, were growing in forests of similar successional stage, but differed  
 913 in mycorrhizal association and consequent resource economic strategies. As stands  
 914 tended to be dominated by trees that associate with arbuscular mycorrhizae (*Frax-*  
 915 *inus* and both *Acer* species made up 70% of total aboveground biomass across  
 916 stands), ecosystem biogeochemical cycle dynamics may be more closely aligned  
 917 to the inorganic nutrient economy proposed in Phillips et al. (2013), which may  
 918 promote stronger nitrogen-water use tradeoffs in tree species that associate with  
 919 arbuscular mycorrhizae. This result was not observed here, as photosynthetic  
 920 properties varied as much within as across the two mycorrhizal associations rep-  
 921 resented. Given the high variability in measured photosynthetic traits within  
 922 and across species, effects of mycorrhizal association likely require more intensive  
 923 sampling efforts to detect than were possible here.

#### 924 3.4.4 *Implications for photosynthetic least-cost theory model development*

925           In the field, soil nutrient availability is heterogeneous across time and space  
 926 (Table S4). Unaccounted within-plot heterogeneity may have contributed to the  
 927 low amount of variation explained by soil N availability in our statistical mod-  
 928 els, as resin bags are a coarse surrogate for soil N availability. Despite this, we  
 929 still observed evidence for nutrient-water use tradeoffs, suggesting that observed  
 930 responses reported here may be an underestimate toward the net effect of soil  
 931 N availability on these tradeoffs. While we urge caution in the interpretation of

932 these results, they do provide a promising baseline for future studies investigating  
933 patterns expected from photosynthetic least-cost theory at finer spatiotemporal  
934 resolutions.

935         The general stronger relationship between leaf N content and photosyn-  
936 thetic parameters versus between leaf N content and soil N availability suggests  
937 that leaf N content is more directly tied to photosynthesis than soil N availabil-  
938 ity. While this could be due to the high spatiotemporal heterogeneity of soil N  
939 availability, principles from photosynthetic least-cost theory suggest that leaf N  
940 content is the downstream product of leaf nutrient demand to build and maintain  
941 photosynthetic machinery, which is set by aboveground environmental conditions  
942 such as light availability, CO<sub>2</sub>, temperature, or vapor pressure deficit (Smith  
943 et al. 2019; Paillassa et al. 2020; Peng et al. 2021; Westerland et al. 2023). The  
944 stronger relationship between leaf N and photosynthetic parameters paired with  
945 the strong negative relationship between leaf N and  $\chi$  could indicate a relatively  
946 stronger effect of climate on leaf N-photosynthesis relationships than soil resource  
947 availability. However, the short distance between plots and across sites limited  
948 our ability to test this mechanism.

949         Variation in soil pH affected least cost responses less than variations in  
950 soil N availability, in part because experimental treatments directly increased soil  
951 N and affected soil pH in opposite directions. While soil pH has been shown  
952 to drive nitrogen-water tradeoffs in global gradient analyses (Viet et al. 2013;  
953 Paillassa et al. 2020), these responses may be due to covariations between soil pH  
954 and nutrient cycling rather than a role of pH per se. The direct manipulations  
955 of soil pH and soil N availability in this study allowed us to partly disentangle



956 these factors and show that variation in N availability matters more for least-cost  
957 tradeoffs than pH alone.

### 958 3.4.5 *Conclusions*

959       Increasing soil N availability generally increased leaf N content (both area-  
960 and mass-based), but did not significantly influence  $\chi$ . This shift in leaf N led  
961 to a reduction in PNUE, and an increase in leaf N per unit  $\chi$  with increasing  
962 soil N availability. Despite null effects of soil N availability on  $\chi$ , we observed a  
963 strong negative relationship between leaf N content and  $\chi$ . These results provide  
964 empirical support for the nutrient-water use tradeoffs expected from photosyn-  
965 thetic least-cost theory in response to soil nutrient availability, but suggest that  
966 all tenets of the theory may not hold in every environment. These results exper-  
967 imentally test previous work suggesting that leaf water-nitrogen economies vary  
968 across gradients of soil nutrient availability and pH, and show that variations in  
969 nutrient availability matter more for determining variation in leaf photosynthetic  
970 traits than soil pH.

971

## Chapter 4

972 The relative cost of resource use for photosynthesis drives variance in  
973 leaf nitrogen content across climate and soil resource availability  
974 gradients

975 4.1 Introduction

976 Terrestrial biosphere models, which comprise the land surface component of  
977 Earth system models, are sensitive to the formulation of photosynthetic processes  
978 (Knorr 2000; Ziehn et al. 2011; Booth et al. 2012). This is because photosynthe-  
979 sis is the largest carbon flux between the atmosphere and terrestrial biosphere,  
980 and is constrained by ecosystem carbon and nutrient cycles (Hungate et al. 2003;  
981 LeBauer and Treseder 2008; IPCC 2021; Fay et al. 2015). Many terrestrial bio-  
982 sphere models formulate photosynthesis by parameterizing photosynthetic capac-  
983 ity within plant functional groups through empirical linear relationships between  
984 area-based leaf nitrogen content ( $N_{\text{area}}$ ) and the maximum carboxylation rate  
985 of Ribulose-1,5-bisphosphate carboxylase/oxygenase (Kattge et al. 2009; Rogers  
986 2014; Rogers et al. 2017). Models are also beginning to include connected carbon-  
987 nitrogen cycles (Wieder et al. 2015; Shi et al. 2016; Davies-Barnard et al. 2020;  
988 Braghiere et al. 2022), which allows leaf photosynthesis to be predicted directly  
989 through changes in  $N_{\text{area}}$  and indirectly through changes in soil nitrogen avail-  
990 ability (e.g., LPJ-GUESS, Smith et al., 2014; CLM5.0, Lawrence et al., 2019).  
991 Despite recent model developments, open questions remain regarding the gen-  
992 erality of ecological relationships between soil nitrogen availability, leaf nitrogen  
993 content, and leaf photosynthesis across edaphic and climatic gradients.

994 Empirical support for positive relationships between soil nitrogen avail-

995 ability and  $N_{\text{area}}$  is abundant (Firn et al. 2019; Liang et al. 2020), and is a  
 996 result often attributed to the high nitrogen cost of building and maintaining Ru-  
 997 bisco (Evans 1989; Evans and Seemann 1989; Onoda et al. 2004; Onoda et al.  
 998 2017; Dong et al. 2020). Such patterns imply that positive relationships between  
 999 soil nitrogen availability and  $N_{\text{area}}$  should cause an increase in leaf photosyn-  
 1000 thesis and photosynthetic capacity by increasing the maximum rate of Rubisco  
 1001 carboxylation through increased investments to Rubisco construction and mainte-  
 1002 nance. This integrated  $N_{\text{area}}$ -photosynthesis response to soil nitrogen availability  
 1003 has been observed both in manipulative experiments and across environmental  
 1004 gradients (Field and Mooney 1986; Evans 1989; Walker et al. 2014; Li et al.  
 1005 2020), and is thought to be driven by ecosystem nitrogen limitation, which lim-  
 1006 its primary productivity globally (LeBauer and Treseder 2008; Fay et al. 2015).  
 1007 However, this response is not consistently observed, as recent studies note vari-  
 1008 able  $N_{\text{area}}$ -photosynthesis relationships across soil nitrogen availability gradients  
 1009 (Liang et al. 2020; Luo et al. 2021) and that aboveground growing conditions  
 1010 (e.g., light availability, temperature, vapor pressure deficit) or species identity  
 1011 traits (e.g., photosynthetic pathway, nitrogen acquisition strategy) may be more  
 1012 important for explaining variance in  $N_{\text{area}}$  and photosynthetic capacity across time  
 1013 and space (Adams et al. 2016; Dong et al. 2017; Dong et al. 2020; Dong et al.  
 1014 2022; Smith et al. 2019; Peng et al. 2021; Westerland et al. 2023).

1015 4.2 Methods

1016 4.3 Results

1017 4.4 Discussion

1018

## Chapter 5

1019   Optimal resource investment to photosynthetic capacity maximizes  
1020       nutrient allocation to whole plant growth under elevated CO<sub>2</sub>

1021   5.1   Introduction

1022       Terrestrial ecosystems are regulated by complex carbon and nitrogen cy-  
1023   cles. As a result, terrestrial biosphere models, which are beginning to include  
1024   coupled carbon and nitrogen cycles (Shi et al. 2016; Davies-Barnard et al. 2020;  
1025   Braghiere et al. 2022), must accurately represent these cycles under different  
1026   environmental scenarios to reliably simulate carbon and nitrogen atmosphere-  
1027   biosphere fluxes Hungate et al. (2003), Prentice et al. (2015).

1028   5.2   Methods

1029   5.3   Results

1030   5.4   Discussion

**1031**

**Chapter 6**

**1032**

**Conclusions**

1033

## References

- 1034     Abrams, M. D. and S. A. Mostoller (1995). Gas exchange, leaf structure and  
 1035         nitrogen in contrasting successional tree species growing in open and under-  
 1036         story sites during a drought. *Tree Physiology* 15(6), 361–370.
- 1037     Adams, M. A., T. L. Turnbull, J. I. Sprent, and N. Buchmann (2016). Legumes  
 1038         are different: Leaf nitrogen, photosynthesis, and water use efficiency. *Pro-  
 1039         ceedings of the National Academy of Sciences of the United States of Amer-  
 1040         ica* 113(15), 4098–4103.
- 1041     Ainsworth, E. A. and S. P. Long (2005). What have we learned from 15 years of  
 1042         free-air CO<sub>2</sub> enrichment (FACE)? A meta-analytic review of the responses  
 1043         of photosynthesis, canopy properties and plant production to rising CO<sub>2</sub>.  
 1044         *New Phytologist* 165(2), 351–372.
- 1045     Allen, K., J. B. Fisher, R. P. Phillips, J. S. Powers, and E. R. Brzostek (2020).  
 1046         Modeling the carbon cost of plant nitrogen and phosphorus uptake across  
 1047         temperate and tropical forests. *Frontiers in Forests and Global Change* 3,  
 1048         1–12.
- 1049     Allison, S. D., C. I. Czimczik, and K. K. Treseder (2008). Microbial activity  
 1050         and soil respiration under nitrogen addition in Alaskan boreal forest. *Global  
 1051         Change Biology* 14(5), 1156–1168.
- 1052     Andersen, M. K., H. Hauggaard-Nielsen, P. Ambus, and E. S. Jensen (2005).  
 1053         Biomass production, symbiotic nitrogen fixation and inorganic N use in dual  
 1054         and tri-component annual intercrops. *Plant and Soil* 266(1-2), 273–287.

- 1055** Arndal, M. F., A. Tolver, K. S. Larsen, C. Beier, and I. K. Schmidt (2018). Fine  
**1056** root growth and vertical distribution in response to elevated CO<sub>2</sub>, warming  
**1057** and drought in a mixed heathland–grassland. *Ecosystems* 21(1), 15–30.
- 1058** Arnone, J. A. (1997). Indices of plant N availability in an alpine grassland under  
**1059** elevated atmospheric CO<sub>2</sub>. *Plant and Soil* 190(1), 61–66.
- 1060** Bae, K., T. J. Fahey, R. D. Yanai, and M. Fisk (2015). Soil nitrogen availabil-  
**1061** ity affects belowground carbon allocation and soil respiration in northern  
**1062** hardwood forests of New Hampshire. *Ecosystems* 18(7), 1179–1191.
- 1063** Bates, D., M. Mächler, B. Bolker, and S. Walker (2015). Fitting linear mixed-  
**1064** effects models using lme4. *Journal of Statistical Software* 67(1), 1–48.
- 1065** Bengtson, P., J. Barker, and S. J. Grayston (2012). Evidence of a strong cou-  
**1066** pling between root exudation, C and N availability, and stimulated SOM  
**1067** decomposition caused by rhizosphere priming effects. *Ecology and Evolu-*  
**1068** *tion* 2(8), 1843–1852.
- 1069** Bernacchi, C. J., E. L. Singsaas, C. Pimentel, A. R. Portis, and S. P. Long  
**1070** (2001). Improved temperature response functions for models of Rubisco-  
**1071** limited photosynthesis. *Plant, Cell and Environment* 24(2), 253–259.
- 1072** Bialic-Murphy, L., N. G. Smith, P. Voothuluru, R. M. McElderry, M. D.  
**1073** Roche, S. T. Cassidy, S. N. Kivlin, and S. Kalisz (2021). Invasion-induced  
**1074** root–fungal disruptions alter plant water and nitrogen economies. *Ecology*  
**1075** *Letters* 24(6), 1145–1156.
- 1076** Bloom, A. J., F. S. Chapin, and H. A. Mooney (1985). Resource limitation  
**1077** in plants - an economic analogy. *Annual Review of Ecology and Systemat-*

- 1078        *ics* 16(1), 363–392.
- 1079        Bonan, G. B., M. D. Hartman, W. J. Parton, and W. R. Wieder (2013). Evaluat-  
 1080        ing litter decomposition in earth system models with long-term litterbag ex-  
 1081        periments: an example using the Community Land Model version 4 (CLM4).  
 1082        *Global Change Biology* 19(3), 957–974.
- 1083        Bonan, G. B., P. J. Lawrence, K. W. Oleson, S. Levis, M. Jung, M. Reich-  
 1084        stein, D. M. Lawrence, and S. C. Swenson (2011). Improving canopy pro-  
 1085        cesses in the Community Land Model version 4 (CLM4) using global flux  
 1086        fields empirically inferred from FLUXNET data. *Journal of Geophysical Re-*  
 1087        *search* 116(G2), G02014.
- 1088        Booth, B. B. B., C. D. Jones, M. Collins, I. J. Totterdell, P. M. Cox, S. Sitch,  
 1089        C. Huntingford, R. A. Betts, G. R. Harris, and J. Lloyd (2012). High sen-  
 1090        sitivity of future global warming to land carbon cycle processes. *Environ-*  
 1091        *mental Research Letters* 7(2), 024002.
- 1092        Borer, E. T., W. S. Harpole, P. B. Adler, E. M. Lind, J. L. Orrock, E. W.  
 1093        Seabloom, and M. D. Smith (2014). Finding generality in ecology: A model  
 1094        for globally distributed experiments. *Methods in Ecology and Evolution* 5(1),  
 1095        65–73.
- 1096        Braghiere, R. K., J. B. Fisher, K. Allen, E. Brzostek, M. Shi, X. Yang, D. M.  
 1097        Ricciuto, R. A. Fisher, Q. Zhu, and R. P. Phillips (2022). Modeling global  
 1098        carbon costs of plant nitrogen and phosphorus acquisition. *Journal of Ad-*  
 1099        *vances in Modeling Earth Systems* 14(8), 1–23.
- 1100        Brix, H. (1971). Effects of nitrogen fertilization on photosynthesis and respira-  
 1101        tion in Douglas-fir. *Forest Science* 17(4), 407–414.



- 1102** Brzostek, E. R., J. B. Fisher, and R. P. Phillips (2014). Modeling the carbon  
**1103** cost of plant nitrogen acquisition: Mycorrhizal trade-offs and multipath  
**1104** resistance uptake improve predictions of retranslocation. *Journal of Geo-*  
**1105** *physical Research: Biogeosciences* 119, 1684–1697.
- 1106** Bubier, J. L., R. Smith, S. Juutinen, T. R. Moore, R. Minocha, S. Long, and  
**1107** S. Minocha (2011). Effects of nutrient addition on leaf chemistry, morphol-  
**1108** ogy, and photosynthetic capacity of three bog shrubs. *Oecologia* 167(2),  
**1109** 355–368.
- 1110** Cernusak, L. A., N. Ubierna, K. Winter, J. A. M. Holtum, J. D. Marshall, and  
**1111** G. D. Farquhar (2013). Environmental and physiological determinants of  
**1112** carbon isotope discrimination in terrestrial plants. *New Phytologist* 200(4),  
**1113** 950–965.
- 1114** Clark, D. B., L. M. Mercado, S. Sitch, C. D. Jones, N. Gedney, M. J. Best,  
**1115** M. Pryor, G. G. Rooney, R. L. H. Essery, E. Blyth, O. Boucher, R. J.  
**1116** Harding, C. Huntingford, and P. M. Cox (2011). The Joint UK Land Envi-  
**1117** ronment Simulator (JULES), model description. Part 2: Carbon fluxes and  
**1118** vegetation dynamics. *Geoscientific Model Development* 4(3), 701–722.
- 1119** Cornwell, W. K., J. H. C. Cornelissen, K. Amatangelo, E. Dorrepaal, V. T.  
**1120** Eviner, O. Godoy, S. E. Hobbie, B. Hoorens, H. Kurokawa, N. Pérez-  
**1121** Harguindeguy, H. M. Quested, L. S. Santiago, D. A. Wardle, I. J. Wright,  
**1122** R. Aerts, S. D. Allison, P. van Bodegom, V. Brovkin, A. Chatain, T. V.  
**1123** Callaghan, S. Díaz, E. Garnier, D. E. Gurvich, E. Kazakou, J. A. Klein,  
**1124** J. Read, P. B. Reich, N. A. Soudzilovskaia, M. V. Vaieretti, and M. Westoby  
**1125** (2008). Plant species traits are the predominant control on litter decompo-

- 1126        sition rates within biomes worldwide. *Ecology Letters* 11(10), 1065–1071.
- 1127        Cornwell, W. K., I. J. Wright, J. Turner, V. Maire, M. M. Barbour, L. A.
- 1128        Cernusak, T. E. Dawson, D. S. Ellsworth, G. D. Farquhar, H. Griffiths,
- 1129        C. Keitel, A. Knohl, P. B. Reich, D. G. Williams, R. Bhaskar, J. H. C. Cor-
- 1130        nelissen, A. Richards, S. Schmidt, F. Valladares, C. Körner, E.-D. Schulze,
- 1131        N. Buchmann, and L. S. Santiago (2018). Climate and soils together regu-
- 1132        late photosynthetic carbon isotope discrimination within C<sub>3</sub> plants worldwide. *Global Ecology and Biogeography* 27(9), 1056–1067.
- 1133
- 1134        Davies-Barnard, T., J. Meyerholt, S. Zaehle, P. Friedlingstein, V. Brovkin,
- 1135        Y. Fan, R. A. Fisher, C. D. Jones, H. Lee, D. Peano, B. Smith, D. Wårilind,
- 1136        and A. J. Wiltshire (2020). Nitrogen cycling in CMIP6 land surface models:
- 1137        progress and limitations. *Biogeosciences* 17(20), 5129–5148.
- 1138        Delaire, M., E. Frak, M. Sigogne, B. Adam, F. Beaujard, and X. Le Roux
- 1139        (2005). Sudden increase in atmospheric CO<sub>2</sub> concentration reveals strong
- 1140        coupling between shoot carbon uptake and root nutrient uptake in young
- 1141        walnut trees. *Tree Physiology* 25(2), 229–235.
- 1142        Doane, T. A. and W. R. Horváth (2003). Spectrophotometric determination of
- 1143        nitrate with a single reagent. *Analytical Letters* 36(12), 2713–2722.
- 1144        Dong, N., I. C. Prentice, B. J. Evans, S. Caddy-Retalic, A. J. Lowe, and I. J.
- 1145        Wright (2017). Leaf nitrogen from first principles: field evidence for adaptive
- 1146        variation with climate. *Biogeosciences* 14(2), 481–495.
- 1147        Dong, N., I. C. Prentice, I. J. Wright, B. J. Evans, H. F. Togashi, S. Caddy-
- 1148        Retalic, F. A. McInerney, B. Sparrow, E. Leitch, and A. J. Lowe (2020).
- 1149        Components of leaf-trait variation along environmental gradients. *New Phy-*

- 1150** *tologist* 228(1), 82–94.
- 1151** Dong, N., I. C. Prentice, I. J. Wright, H. Wang, O. K. Atkin, K. J. Bloomfield,  
**1152** T. F. Domingues, S. M. Gleason, V. Maire, Y. Onoda, H. Poorter, and N. G.  
**1153** Smith (2022). Leaf nitrogen from the perspective of optimal plant function.  
**1154** *Journal of Ecology* 110(11), 2585–2602.
- 1155** Dovrat, G., H. Bakhshian, T. Masci, and E. Sheffer (2020). The nitrogen eco-  
**1156** nomic spectrum of legume stoichiometry and fixation strategy. *New Phytol-*  
**1157** *ogist* 227(2), 365–375.
- 1158** Dovrat, G., T. Masci, H. Bakhshian, E. Mayzlish Gati, S. Golan, and E. Shef-  
**1159** fer (2018). Drought-adapted plants dramatically downregulate dinitrogen  
**1160** fixation: Evidences from Mediterranean legume shrubs. *Journal of Ecol-*  
**1161** *ogy* 106(4), 1534–1544.
- 1162** Duursma, R. A. (2015). Plantecophys - An R Package for Analysing and Mod-  
**1163** elling Leaf Gas Exchange Data. *PLOS ONE* 10(11), e0143346.
- 1164** Eastman, B. A., M. B. Adams, E. R. Brzostek, M. B. Burnham, J. E. Carrara,  
**1165** C. Kelly, B. E. McNeil, C. A. Walter, and W. T. Peterjohn (2021). Altered  
**1166** plant carbon partitioning enhanced forest ecosystem carbon storage after 25  
**1167** years of nitrogen additions. *New Phytologist* 230(4), 1435–1448.
- 1168** Ellsworth, D. S. and P. B. Reich (1996). Photosynthesis and leaf nitrogen in five  
**1169** Amazonian tree species during early secondary succession. *Ecology* 77(2),  
**1170** 581–594.
- 1171** Espelta, J. M., P. Cortés, M. Mangirón, and J. Retana (2005). Differences in  
**1172** biomass partitioning, leaf nitrogen content, and water use efficiency d13C

- 1173 result in similar performance of seedlings of two Mediterranean oaks with  
 1174 contrasting leaf habit. *Ecoscience* 12(4), 447–454.
- 1175 Evans, J. R. (1989). Photosynthesis and nitrogen relationships in leaves of C<sub>3</sub>  
 1176 plants. *Oecologia* 78(1), 9–19.
- 1177 Evans, J. R. and H. Poorter (2001). Photosynthetic acclimation of plants to  
 1178 growth irradiance: the relative importance of specific leaf area and nitrogen  
 1179 partitioning in maximizing carbon gain. *Plant, Cell and Environment* 24(8),  
 1180 755–767.
- 1181 Evans, J. R. and J. R. Seemann (1989). The allocation of protein nitrogen in  
 1182 the photosynthetic apparatus: costs, consequences, and control. *Photosyn-*  
 1183 *thesis* 8, 183–205.
- 1184 Exbrayat, J.-F., A. A. Bloom, P. Falloon, A. Ito, T. L. Smallman, and  
 1185 M. Williams (2018). Reliability ensemble averaging of 21<sup>st</sup> century projec-  
 1186 tions of terrestrial net primary productivity reduces global and regional  
 1187 uncertainties. *Earth System Dynamics* 9(1), 153–165.
- 1188 Farquhar, G. D., J. R. Ehleringer, and K. T. Hubick (1989). Carbon Isotope  
 1189 Discrimination and Photosynthesis. *Annual Review of Plant Physiology and*  
 1190 *Plant Molecular Biology* 40(1), 503–537.
- 1191 Farquhar, G. D., S. von Caemmerer, and J. A. Berry (1980). A biochem-  
 1192 ical model of photosynthetic CO<sub>2</sub> assimilation in leaves of C<sub>3</sub> species.  
 1193 *Planta* 149(1), 78–90.
- 1194 Fay, P. A., S. M. Prober, W. S. Harpole, J. M. H. Knops, J. D. Bakker, E. T.  
 1195 Borer, E. M. Lind, A. S. MacDougall, E. W. Seabloom, P. D. Wragg, P. B.

- 1196** Adler, D. M. Blumenthal, Y. M. Buckley, C. Chu, E. E. Cleland, S. L.  
**1197** Collins, K. F. Davies, G. Du, X. Feng, J. Firn, D. S. Gruner, N. Hagenah,  
**1198** Y. Hautier, R. W. Heckman, V. L. Jin, K. P. Kirkman, J. A. Klein, L. M.  
**1199** Ladwig, Q. Li, R. L. McCulley, B. A. Melbourne, C. E. Mitchell, J. L. Moore,  
**1200** J. W. Morgan, A. C. Risch, M. Schütz, C. J. Stevens, D. A. Wedin, and  
**1201** L. H. Yang (2015). Grassland productivity limited by multiple nutrients.  
**1202** *Nature Plants* 1(7), 15080.
- 1203** Field, C. B. and H. A. Mooney (1986). The photosynthesis-nitrogen relationship  
**1204** in wild plants. In T. J. Givnish (Ed.), *On the Economy of Plant Form and*  
**1205** *Function*, pp. 25–55. Cambridge: Cambridge University Press.
- 1206** Firn, J., J. M. McGree, E. Harvey, H. Flores Moreno, M. Schutz, Y. M. Buckley,  
**1207** E. T. Borer, E. W. Seabloom, K. J. La Pierre, A. M. MacDougall, S. M.  
**1208** Prober, C. J. Stevens, L. L. Sullivan, E. Porter, E. Ladouceur, C. Allen,  
**1209** K. H. Moromizato, J. W. Morgan, W. S. Harpole, Y. Hautier, N. Eisen-  
**1210** hauer, J. P. Wright, P. B. Adler, C. A. Arnillas, J. D. Bakker, L. Biederman,  
**1211** A. A. D. Broadbent, C. S. Brown, M. N. Bugalho, M. C. Caldeira, E. E. Cle-  
**1212** land, A. Ebeling, P. A. Fay, N. Hagenah, A. R. Kleinhesselink, R. Mitchell,  
**1213** J. L. Moore, C. Nogueira, P. L. Peri, C. Roscher, M. D. Smith, P. D. Wragg,  
**1214** and A. C. Risch (2019). Leaf nutrients, not specific leaf area, are consistent  
**1215** indicators of elevated nutrient inputs. *Nature Ecology and Evolution* 3(3),  
**1216** 400–406.
- 1217** Fisher, J. B., S. Sitch, Y. Malhi, R. A. Fisher, C. Huntingford, and S.-Y. Tan  
**1218** (2010). Carbon cost of plant nitrogen acquisition: A mechanistic, globally  
**1219** applicable model of plant nitrogen uptake, retranslocation, and fixation.

- 1220        *Global Biogeochemical Cycles* 24(1), 1–17.
- 1221        Fox, J. and S. Weisberg (2019). *An R companion to applied regression* (Third
- 1222        edit ed.). Thousand Oaks, California: Sage.
- 1223        Franklin, O., R. E. McMurtrie, C. M. Iversen, K. Y. Crous, A. C. Finzi, D. Tis-
- 1224        sue, D. S. Ellsworth, R. Oren, and R. J. Norby (2009). Forest fine-root
- 1225        production and nitrogen use under elevated CO<sub>2</sub>: contrasting responses
- 1226        in evergreen and deciduous trees explained by a common principle. *Global*
- 1227        *Change Biology* 15(1), 132–144.
- 1228        Friedlingstein, P., M. Meinshausen, V. K. Arora, C. D. Jones, A. Anav, S. K.
- 1229        Liddicoat, and R. Knutti (2014). Uncertainties in CMIP5 climate projections
- 1230        due to carbon cycle feedbacks. *Journal of Climate* 27(2), 511–526.
- 1231        Friel, C. A. and M. L. Friesen (2019). Legumes modulate allocation to rhizobial
- 1232        nitrogen fixation in response to factorial light and nitrogen manipulation.
- 1233        *Frontiers in Plant Science* 10, 1316.
- 1234        Fujikake, H., A. Yamazaki, N. Ohtake, K. Sueoshi, S. Matsushashi, T. Ito,
- 1235        C. Mizuniwa, T. Kume, S. Hoshimoto, N.-S. Ishioka, S. Watanabe, A. Osa,
- 1236        T. Sekine, H. Uchida, A. Tsuji, and T. Ohyama (2003). Quick and reversible
- 1237        inhibition of soybean root nodule growth by nitrate involves a decrease in
- 1238        sucrose supply to nodules. *Journal of Experimental Botany* 54(386), 1379–
- 1239        1388.
- 1240        Ghimire, B., W. J. Riley, C. D. Koven, J. Kattge, A. Rogers, P. B. Reich, and
- 1241        I. J. Wright (2017). A global trait-based approach to estimate leaf nitro-
- 1242        gen functional allocation from observations:. *Ecological Applications* 27(5),
- 1243        1421–1434.

- 1244 Giardina, C. P., M. D. Coleman, J. E. Hancock, J. S. King, E. A. Lilleskov,  
1245 W. M. Loya, K. S. Pregitzer, M. G. Ryan, and C. C. Trettin (2005). The  
1246 response of belowground carbon allocation in forests to global change. In  
1247 D. Binkley and O. Manyilo (Eds.), *Tree Species Effects on Soils: Implica-*  
1248 *tions for Global Change* (Volume 55 ed.), Chapter Chapter 7, pp. 119–154.  
1249 Berlin/Heidelberg: Springer-Verlag.
- 1250 Gibson, A. H. and J. E. Harper (1985). Nitrate effect on nodulation of soybean  
1251 by *Bradyrhizobium japonicum*. *Crop Science* 25(3), 497–501.
- 1252 Gill, A. L. and A. C. Finzi (2016). Belowground carbon flux links biogeochemical  
1253 cycles and resource-use efficiency at the global scale. *Ecology Letters* 19(12),  
1254 1419–1428.
- 1255 Goll, D. S., V. Brovkin, B. R. Parida, C. H. Reick, J. Kattge, P. B. Reich, P. M.  
1256 van Bodegom, and Ü. Niinemets (2012). Nutrient limitation reduces land  
1257 carbon uptake in simulations with a model of combined carbon, nitrogen  
1258 and phosphorus cycling. *Biogeosciences Discussions* 9(3), 3173–3232.
- 1259 Gregory, L. M., A. M. McClain, D. M. Kramer, J. D. Pardo, K. E. Smith, O. L.  
1260 Tessmer, B. J. Walker, L. G. Ziccardi, and T. D. Sharkey (2021, oct). The  
1261 triose phosphate utilization limitation of photosynthetic rate: Out of global  
1262 models but important for leaf models. *Plant, Cell and Environment* 44(10),  
1263 3223–3226.
- 1264 Guerrieri, R., M. Mencuccini, L. J. Sheppard, M. Saurer, M. P. Perks, P. Levy,  
1265 M. A. Sutton, M. Borghetti, and J. Grace (2011). The legacy of enhanced  
1266 N and S deposition as revealed by the combined analysis of  $\delta^{13}\text{C}$ ,  $\delta^{18}\text{O}$  and  
1267  $\delta^{15}\text{N}$  in tree rings. *Global Change Biology* 17(5), 1946–1962.

- 1268 Gulmon, S. L. and C. C. Chu (1981). The effects of light and nitrogen on pho-  
1269 tosynthesis, leaf characteristics, and dry matter allocation in the chaparral  
1270 shrub, *Diplacus aurantiacus*. *Oecologia* 49(2), 207–212.
- 1271 Gutschick, V. P. (1981). Evolved strategies in nitrogen acquisition by plants.  
1272 *The American Naturalist* 118(5), 607–637.
- 1273 Hallik, L., Ü. Niinemets, and I. J. Wright (2009). Are species shade and drought  
1274 tolerance reflected in leaf-level structural and functional differentiation in  
1275 Northern Hemisphere temperate woody flora? *New Phytologist* 184(1), 257–  
1276 274.
- 1277 Harrison, M. T., E. J. Edwards, G. D. Farquhar, A. B. Nicotra, and J. R.  
1278 Evans (2009). Nitrogen in cell walls of sclerophyllous leaves accounts for  
1279 little of the variation in photosynthetic nitrogen-use efficiency. *Plant, Cell*  
1280 *and Environment* 32(3), 259–270.
- 1281 Harrison, S. P., W. Cramer, O. Franklin, I. C. Prentice, H. Wang,  
1282 Å. Brännström, H. de Boer, U. Dieckmann, J. Joshi, T. F. Keenan,  
1283 A. Lavergne, S. Manzoni, G. Mengoli, C. Morfopoulos, J. Peñuelas,  
1284 S. Pietsch, K. T. Rebel, Y. Ryu, N. G. Smith, B. D. Stocker, and I. J.  
1285 Wright (2021). Eco-evolutionary optimality as a means to improve vegeta-  
1286 tion and land-surface models. *New Phytologist* 231(6), 2125–2141.
- 1287 Henneron, L., P. Kardol, D. A. Wardle, C. Cros, and S. Fontaine (2020). Rhizo-  
1288 sphere control of soil nitrogen cycling: a key component of plant economic  
1289 strategies. *New Phytologist* 228(4), 1269–1282.
- 1290 Hikosaka, K. and A. Shigeno (2009). The role of Rubisco and cell walls in the  
1291 interspecific variation in photosynthetic capacity. *Oecologia* 160(3), 443–



- 1292** 451.
- 1293** Hoagland, D. R. and D. I. Arnon (1950). The water culture method for growing  
**1294** plants without soil. *California Agricultural Experiment Station: 347* 347(2),  
**1295** 1–32.
- 1296** Hobbie, E. A. (2006). Carbon allocation to ectomycorrhizal fungi correlates  
**1297** with belowground allocation in culture studies. *Ecology* 87(3), 563–569.
- 1298** Hobbie, E. A. and J. E. Hobbie (2008). Natural abundance of  $^{15}\text{N}$  in nitrogen-  
**1299** limited forests and tundra can estimate nitrogen cycling through mycorrhizal  
**1300** fungi: a review. *Ecosystems* 11(5), 815–830.
- 1301** Hoek, T. A., K. Axelrod, T. Biancalani, E. A. Yurtsev, J. Liu, and J. Gore  
**1302** (2016). Resource availability modulates the cooperative and competitive na-  
**1303** ture of a microbial cross-feeding mutualism. *PLOS Biology* 14(8), e1002540.
- 1304** Högberg, M. N., M. J. I. Briones, S. G. Keel, D. B. Metcalfe, C. Campbell, A. J.  
**1305** Midwood, B. Thornton, V. Hurry, S. Linder, T. Näsholm, and P. Högberg  
**1306** (2010). Quantification of effects of season and nitrogen supply on tree below-  
**1307** ground carbon transfer to ectomycorrhizal fungi and other soil organisms in  
**1308** a boreal pine forest. *New Phytologist* 187(2), 485–493.
- 1309** Högberg, P., M. N. Högberg, S. G. Göttlicher, N. R. Betson, S. G. Keel, D. B.  
**1310** Metcalfe, C. Campbell, A. Schindlbacher, V. Hurry, T. Lundmark, S. Linder,  
**1311** and T. Näsholm (2008). High temporal resolution tracing of photosynthate  
**1312** carbon from the tree canopy to forest soil microorganisms. *New Phytolo-*  
**1313** *gist* 177(1), 220–228.
- 1314** Houlton, B. Z., Y.-P. Wang, P. M. Vitousek, and C. B. Field (2008). A uni-

- 1315        fying framework for dinitrogen fixation in the terrestrial biosphere. *Nature*
- 1316        *454*(7202), 327–330.
- 1317        Hungate, B. A., J. S. Dukes, M. R. Shaw, Y. Luo, and C. B. Field (2003).
- 1318        Nitrogen and climate change. *Science* *302*(5650), 1512–1513.
- 1319        IPCC (2021). *Climate Change 2021: The Physical Science Basis. Contribution*
- 1320        *of Working Group I to the Sixth Assessment Report of the Intergovernmental*
- 1321        *Panel on Climate Change*. Cambridge University Press.
- 1322        Johnson, N. C., J. H. Graham, and F. A. Smith (1997). Functioning of mycor-
- 1323        rhizal associations along the mutualism-parasitism continuum. *New Phytol-*
- 1324        *ogist* *135*(4), 575–585.
- 1325        Kaiser, C., M. R. Kilburn, P. L. Clode, L. Fuchslueger, M. Koranda, J. B. Cliff,
- 1326        Z. M. Solaiman, and D. V. Murphy (2015). Exploring the transfer of recent
- 1327        plant photosynthates to soil microbes: mycorrhizal pathway vs direct root
- 1328        exudation. *New Phytologist* *205*(4), 1537–1551.
- 1329        Katabuchi, M. (2015). LeafArea: An R package for rapid digital analysis of leaf
- 1330        area. *Ecological Research* *30*(6), 1073–1077.
- 1331        Kattge, J. and W. Knorr (2007). Temperature acclimation in a biochemical
- 1332        model of photosynthesis: a reanalysis of data from 36 species. *Plant, Cell*
- 1333        *and Environment* *30*(9), 1176–1190.
- 1334        Kattge, J., W. Knorr, T. Raddatz, and C. Wirth (2009). Quantifying photosyn-
- 1335        thetic capacity and its relationship to leaf nitrogen content for global-scale
- 1336        terrestrial biosphere models. *Global Change Biology* *15*(4), 976–991.
- 1337        Kayler, Z., A. Gessler, and N. Buchmann (2010). What is the speed of link

- 1338        between aboveground and belowground processes? *New Phytologist* 187(4),  
1339        885–888.
- 1340        Kayler, Z., C. Keitel, K. Jansen, and A. Gessler (2017). Experimental evi-  
1341        dence of two mechanisms coupling leaf-level C assimilation to rhizosphere  
1342        CO<sub>2</sub> release. *Environmental and Experimental Botany* 135,  
1343        21–26.
- 1344        Keeling, C. D., W. G. Mook, and P. P. Tans (1979, jan). Recent trends in the  
1345        <sup>13</sup>C/<sup>12</sup>C ratio of atmospheric carbon dioxide.  
1346        *Nature* 277(5692), 121–123.
- 1347        Kenward, M. G. and J. H. Roger (1997). Small sample inference for fixed effects  
1348        from restricted maximum likelihood. *Biometrics* 53(3), 983.
- 1349        Knapp, A. K., M. L. Avolio, C. Beier, C. J. W. Carroll, S. L. Collins, J. S.  
1350        Dukes, L. H. Fraser, R. J. Griffin-Nolan, D. L. Hoover, A. Jentsch, M. E.  
1351        Loik, R. P. Phillips, A. K. Post, O. E. Sala, I. J. Slette, L. Yahdjian, and  
1352        M. D. Smith (2017). Pushing precipitation to the extremes in distributed  
1353        experiments: recommendations for simulating wet and dry years. *Global*  
1354        *Change Biology* 23(5), 1774–1782.
- 1355        Knorr, W. (2000). Annual and interannual CO<sub>2</sub> exchanges of the  
1356        terrestrial biosphere: process-based simulations and uncertainties. *Global*  
1357        *Ecology and Biogeography* 9(3), 225–252.
- 1358        Knorr, W. and M. Heimann (2001). Uncertainties in global terrestrial biosphere  
1359        modeling: 1. A comprehensive sensitivity analysis with a new photosynthesis  
1360        and energy balance scheme. *Global Biogeochemical Cycles* 15(1), 207–225.

- 1361** Kulmatiski, A., P. B. Adler, J. M. Stark, and A. T. Tredennick (2017). Water  
**1362** and nitrogen uptake are better associated with resource availability than  
**1363** root biomass. *Ecosphere* 8(3), e01738.
- 1364** Lawrence, D. M., R. A. Fisher, C. D. Koven, K. W. Oleson, S. C. Swen-  
**1365** son, G. B. Bonan, N. Collier, B. Ghimire, L. Kampenhout, D. Kennedy,  
**1366** E. Kluzek, P. J. Lawrence, F. Li, H. Li, D. L. Lombardozzi, W. J. Riley,  
**1367** W. J. Sacks, M. Shi, M. Vertenstein, W. R. Wieder, C. Xu, A. A. Ali,  
**1368** A. M. Badger, G. Bisht, M. Broeke, M. A. Brunke, S. P. Burns, J. Buzan,  
**1369** M. Clark, A. Craig, K. M. Dahlin, B. Drewniak, J. B. Fisher, M. Flanner,  
**1370** A. M. Fox, P. Gentine, F. M. Hoffman, G. Keppel-Aleks, R. Knox, S. Ku-  
**1371** mar, J. Lenaerts, L. R. Leung, W. H. Lipscomb, Y. Lu, A. Pandey, J. D.  
**1372** Pelletier, J. Perket, J. T. Randerson, D. M. Ricciuto, B. M. Sanderson,  
**1373** A. Slater, Z. M. Subin, J. Tang, R. Q. Thomas, M. Val Martin, and X. Zeng  
**1374** (2019). The Community Land Model Version 5: description of new features,  
**1375** benchmarking, and impact of forcing uncertainty. *Journal of Advances in*  
**1376** *Modeling Earth Systems* 11(12), 4245–4287.
- 1377** LeBauer, D. S. and K. K. Treseder (2008). Nitrogen limitation of net primary  
**1378** productivity. *Ecology* 89(2), 371–379.
- 1379** Lenth, R. (2019). emmeans: estimated marginal means, aka least-squares  
**1380** means.
- 1381** Li, W., H. Zhang, G. Huang, R. Liu, H. Wu, C. Zhao, and N. G. McDowell  
**1382** (2020). Effects of nitrogen enrichment on tree carbon allocation: A global  
**1383** synthesis. *Global Ecology and Biogeography* 29(3), 573–589.
- 1384** Liang, J., X. Qi, L. Souza, and Y. Luo (2016). Processes regulating progressive

- 1385** nitrogen limitation under elevated carbon dioxide: a meta-analysis. *Biogeo-*  
**1386** *sciences* 13(9), 2689–2699.
- 1387** Liang, X., T. Zhang, X. Lu, D. S. Ellsworth, H. BassiriRad, C. You, D. Wang,  
**1388** P. He, Q. Deng, H. Liu, J. Mo, and Q. Ye (2020). Global response patterns of  
**1389** plant photosynthesis to nitrogen addition: A meta-analysis. *Global Change*  
**1390** *Biology* 26(6), 3585–3600.
- 1391** Luo, X., T. F. Keenan, J. M. Chen, H. Croft, I. C. Prentice, N. G. Smith,  
**1392** A. P. Walker, H. Wang, R. Wang, C. Xu, and Y. Zhang (2021). Global  
**1393** variation in the fraction of leaf nitrogen allocated to photosynthesis. *Nature*  
**1394** *Communications* 12(1), 4866.
- 1395** Luo, Y., W. S. Currie, J. S. Dukes, A. C. Finzi, U. A. Hartwig, B. A. Hungate,  
**1396** R. E. McMurtrie, R. Oren, W. J. Parton, D. E. Pataki, R. M. Shaw, D. R.  
**1397** Zak, and C. B. Field (2004). Progressive nitrogen limitation of ecosystem  
**1398** responses to rising atmospheric carbon dioxide. *BioScience* 54(8), 731–739.
- 1399** Markham, J. H. and C. Zekveld (2007). Nitrogen fixation makes biomass al-  
**1400** location to roots independent of soil nitrogen supply. *Canadian Journal of*  
**1401** *Botany* (9), 787–793.
- 1402** Matamala, R. and W. H. Schlesinger (2000). Effects of elevated atmospheric  
**1403** CO<sub>2</sub> on fine root production and activity in an intact tem-  
**1404** perate forest ecosystem. *Global Change Biology* 6(8), 967–979.
- 1405** Medlyn, B. E., E. Dreyer, D. S. Ellsworth, M. Forstreuter, P. C. Harley,  
**1406** M. U. F. Kirschbaum, X. Le Roux, P. Montpied, J. Strassmeyer, A. Wal-  
**1407** croft, K. Wang, and D. Loustau (2002). Temperature response of parameters  
**1408** of a biochemically based model of photosynthesis. II. A review of experimen-

- 1409 tal data. *Plant, Cell and Environment* 25(9), 1167–1179.
- 1410 Menge, D. N. L., S. A. Levin, and L. O. Hedin (2008). Evolutionary tradeoffs can  
1411 select against nitrogen fixation and thereby maintain nitrogen limitation.  
1412 *Proceedings of the National Academy of Sciences* 105(5), 1573–1578.
- 1413 Menne, M. J., I. Durre, R. S. Vose, B. E. Gleason, and T. G. Houston (2012).  
1414 An overview of the global historical climatology network-daily database.  
1415 *Journal of Atmospheric and Oceanic Technology* 29(7), 897–910.
- 1416 Meyerholt, J., S. Zaehle, and M. J. Smith (2016). Variability of pro-  
1417 jected terrestrial biosphere responses to elevated levels of atmospheric  
1418 CO<sub>2</sub> due to uncertainty in biological nitrogen fixation. *Bio-  
1419 geosciences* 13(5), 1491–1518.
- 1420 Minocha, R., S. Long, A. H. Magill, J. D. Aber, and W. H. McDowell (2000).  
1421 Foliar free polyamine and inorganic ion content in relation to soil and soil  
1422 solution chemistry in two fertilized forest stands at the Harvard Forest,  
1423 Massachusetts. *Plant and Soil* 222(1-2), 119–137.
- 1424 Muñoz, N., X. Qi, M. W. Li, M. Xie, Y. Gao, M. Y. Cheung, F. L. Wong, and  
1425 H.-M. Lam (2016). Improvement in nitrogen fixation capacity could be part  
1426 of the domestication process in soybean. *Heredity* 117(2), 84–93.
- 1427 Nadelhoffer, K. J. and J. W. Raich (1992). Fine root production estimates and  
1428 belowground carbon allocation in forest ecosystems. *Ecology* 73(4), 1139–  
1429 1147.
- 1430 Niinemets, Ü. and J. D. Tenhunen (1997). A model separating leaf struc-  
1431 tural and physiological effects on carbon gain along light gradients for the

- 1432 shade-tolerant species *Acer saccharum*. *Plant, Cell and Environ-*  
 1433 *ment* 20(7), 845–866.
- 1434 Norby, R. J., J. Ledford, C. D. Reilly, N. E. Miller, and E. G. O'Neill  
 1435 (2004). Fine-root production dominates response of a deciduous forest to  
 1436 atmospheric CO<sub>2</sub> enrichment. *Proceedings of the National Academy of Sci-*  
 1437 *ences* 101(26), 9689–9693.
- 1438 Noyce, G. L., M. L. Kirwan, R. L. Rich, and J. P. Megonigal (2019). Asyn-  
 1439 chronous nitrogen supply and demand produce nonlinear plant allocation  
 1440 responses to warming and elevated CO<sub>2</sub>. *Proceedings of the*  
 1441 *National Academy of Sciences* 116(43), 21623–21628.
- 1442 Onoda, Y., K. Hikosaka, and T. Hirose (2004). Allocation of nitrogen to  
 1443 cell walls decreases photosynthetic nitrogen-use efficiency. *Functional Ecol-*  
 1444 *ogy* 18(3), 419–425.
- 1445 Onoda, Y., I. J. Wright, J. R. Evans, K. Hikosaka, K. Kitajima, Ü. Niinemets,  
 1446 H. Poorter, T. Tosens, and M. Westoby (2017). Physiological and structural  
 1447 tradeoffs underlying the leaf economics spectrum. *New Phytologist* 214(4),  
 1448 1447–1463.
- 1449 Paillassa, J., I. J. Wright, I. C. Prentice, S. Pepin, N. G. Smith, G. Ethier,  
 1450 A. C. Westerband, L. J. Lamarque, H. Wang, W. K. Cornwell, and V. Maire  
 1451 (2020). When and where soil is important to modify the carbon and water  
 1452 economy of leaves. *New Phytologist* 228(1), 121–135.
- 1453 Parvin, S., S. Uddin, S. Tausz Posch, R. Armstrong, and M. Tausz (2020). Car-  
 1454 bon sink strength of nodules but not other organs modulates photosynthesis  
 1455 of faba bean (*Vicia faba*) grown under elevated [CO<sub>2</sub>] and different

- 1456 water supply. *New Phytologist* 227(1), 132–145.
- 1457 Peng, Y., K. J. Bloomfield, L. A. Cernusak, T. F. Domingues, and I. C. Pren-  
1458 tice (2021). Global climate and nutrient controls of photosynthetic capacity.  
1459 *Communications Biology* 4(1), 462.
- 1460 Perkowski, E. A., E. F. Waring, and N. G. Smith (2021). Root mass carbon  
1461 costs to acquire nitrogen are determined by nitrogen and light availabil-  
1462 ity in two species with different nitrogen acquisition strategies. *Journal of*  
1463 *Experimental Botany* 72(15), 5766–5776.
- 1464 Phillips, R. P., E. R. Brzostek, and M. G. Midgley (2013). The mycorrhizal-  
1465 associated nutrient economy: a new framework for predicting carbon-  
1466 nutrient couplings in temperate forests. *New Phytologist* 199(1), 41–51.
- 1467 Phillips, R. P., A. C. Finzi, and E. S. Bernhardt (2011). Enhanced root ex-  
1468 udation induces microbial feedbacks to N cycling in a pine forest under  
1469 long-term CO<sub>2</sub> fumigation. *Ecology Letters* 14(2), 187–194.
- 1470 Pons, T. L. and R. W. Pearcy (1994). Nitrogen reallocation and photosynthetic  
1471 acclimation in response to partial shading in soybean plants. *Physiologia*  
1472 *Plantarum* 92(4), 636–644.
- 1473 Poorter, H., J. Bühler, D. Van Dusschoten, J. Climent, and J. A. Postma (2012).  
1474 Pot size matters: A meta-analysis of the effects of rooting volume on plant  
1475 growth. *Functional Plant Biology* 39(11), 839–850.
- 1476 Prentice, I. C., N. Dong, S. M. Gleason, V. Maire, and I. J. Wright (2014).  
1477 Balancing the costs of carbon gain and water transport: testing a new theo-  
1478 retical framework for plant functional ecology. *Ecology Letters* 17(1), 82–91.



- 1479 Prentice, I. C., X. Liang, B. E. Medlyn, and Y.-P. Wang (2015). Reliable, ro-  
 1480 bust and realistic: The three R's of next-generation land-surface modelling.  
 1481 *Atmospheric Chemistry and Physics* 15, 5987–6005.
- 1482 Querejeta, J. I., I. Prieto, C. Armas, F. Casanoves, J. S. Diémé, M. Diouf,  
 1483 H. Yossi, B. Kaya, F. I. Pugnaire, and G. M. Rusch (2022). Higher leaf  
 1484 nitrogen content is linked to tighter stomatal regulation of transpiration  
 1485 and more efficient water use across dryland trees. *New Phytologist* 235(4),  
 1486 1351–1364.
- 1487 R Core Team (2021). R: A language and environment for statistical computing.
- 1488 Raich, J. W., D. A. Clark, L. Schwendenmann, and T. E. Wood (2014). Above-  
 1489 ground tree growth varies with belowground carbon allocation in a tropical  
 1490 rainforest environment. *PLoS ONE* 9(6), e100275.
- 1491 Rastetter, E. B., P. M. Vitousek, C. B. Field, G. R. Shaver, D. Herbert, and  
 1492 G. I. Ågren (2001). Resource optimization and symbiotic nitrogen fixation.  
 1493 *Ecosystems* 4(4), 369–388.
- 1494 Reich, P. B. (2014). The world-wide 'fast-slow' plant economics spectrum: a  
 1495 traits manifesto. *Journal of Ecology* 102(2), 275–301.
- 1496 Rhine, E. D., R. L. Mulvaney, E. J. Pratt, and G. K. Sims (1998). Improving  
 1497 the Berthelot reaction for determining ammonium in soil extracts and water.  
 1498 *Soil Science Society of America Journal* 62(2), 473.
- 1499 Rogers, A. (2014). The use and misuse of  $V_{c,max}$  in Earth Sys-  
 1500 tem Models. *Photosynthesis Research* 119(1-2), 15–29.
- 1501 Rogers, A., B. E. Medlyn, J. S. Dukes, G. B. Bonan, S. Caemmerer, M. C.

- 1502** Dietze, J. Kattge, A. D. B. Leakey, L. M. Mercado, Ü. Niinemets, I. C.  
**1503** Prentice, S. P. Serbin, S. Sitch, D. A. Way, and S. Zaehle (2017). A roadmap  
**1504** for improving the representation of photosynthesis in Earth system models.  
**1505** *New Phytologist* 213(1), 22–42.
- 1506** Saleh, A. M., M. Abdel-Mawgoud, A. R. Hassan, T. H. Habeeb, R. S. Yehia,  
**1507** and H. AbdElgawad (2020). Global metabolic changes induced by arbuscular  
**1508** mycorrhizal fungi in oregano plants grown under ambient and elevated levels  
**1509** of atmospheric CO<sub>2</sub>. *Plant Physiology and Biochemistry* 151, 255–263.
- 1510** Schaefer, K., C. R. Schwalm, C. Williams, M. A. Arain, A. Barr, J. M. Chen,  
**1511** K. J. Davis, D. Dimitrov, T. W. Hilton, D. Y. Hollinger, E. Humphreys,  
**1512** B. Poulter, B. M. Raczka, A. D. Richardson, A. Sahoo, P. Thornton, R. Var-  
**1513** gas, H. Verbeeck, R. Anderson, I. Baker, T. A. Black, P. Bolstad, J. Chen,  
**1514** P. S. Curtis, A. R. Desai, M. C. Dietze, D. Dragoni, C. M. Gough, R. F.  
**1515** Grant, L. Gu, A. K. Jain, C. Kucharik, B. E. Law, S. Liu, E. Lokipitiya,  
**1516** H. A. Margolis, R. Matamala, J. H. McCaughey, R. Monson, J. W. Munger,  
**1517** W. Oechel, C. Peng, D. T. Price, D. Ricciuto, W. J. Riley, N. Roulet,  
**1518** H. Tian, C. Tonitto, M. Torn, E. Weng, and X. Zhou (2012). A model-  
**1519** data comparison of gross primary productivity: Results from the North  
**1520** American Carbon Program site synthesis. *Journal of Geophysical Research:*  
**1521** *Biogeosciences* 117(G3), G03010.
- 1522** Schneider, C. A., W. S. Rasband, and K. W. Eliceiri (2012). NIH Image to  
**1523** ImageJ: 25 years of image analysis. *Nature Methods* 9(7), 671–675.
- 1524** Scott, H. G. and N. G. Smith (2022). A Model of C4 Photosynthetic Acclimation  
**1525** Based on Least-Cost Optimality Theory Suitable for Earth System Model

- 1526       Incorporation. *Journal of Advances in Modeling Earth Systems* 14(3), 1–16.
- 1527       Shi, M., J. B. Fisher, E. R. Brzostek, and R. P. Phillips (2016). Carbon cost
- 1528       of plant nitrogen acquisition: Global carbon cycle impact from an improved
- 1529       plant nitrogen cycle in the Community Land Model. *Global Change Biol-*
- 1530       *ogy* 22(3), 1299–1314.
- 1531       Shi, M., J. B. Fisher, R. P. Phillips, and E. R. Brzostek (2019). Neglecting
- 1532       plant–microbe symbioses leads to underestimation of modeled climate im-
- 1533       pacts. *Biogeosciences* 16(2), 457–465.
- 1534       Smith, N. G. and J. S. Dukes (2013). Plant respiration and photosynthesis in
- 1535       global-scale models: incorporating acclimation to temperature and CO<sub>2</sub>.
- 1536       *Global Change Biology* 19(1), 45–63.
- 1537       Smith, N. G., T. F. Keenan, I. C. Prentice, H. Wang, I. J. Wright, Ü. Niinemets,
- 1538       K. Y. Crous, T. F. Domingues, R. Guerrieri, F. Ito, J. Kattge, E. L.
- 1539       Kruger, V. Maire, A. Rogers, S. P. Serbin, L. Tarvainen, H. F. Togashi,
- 1540       P. A. Townsend, M. Wang, L. K. Weerasinghe, and S.-X. Zhou (2019).
- 1541       Global photosynthetic capacity is optimized to the environment. *Ecology*
- 1542       *Letters* 22(3), 506–517.
- 1543       Smith, N. G., D. L. Lombardozzi, A. Tawfik, G. B. Bonan, and J. S. Dukes
- 1544       (2017). Biophysical consequences of photosynthetic temperature acclimation
- 1545       for climate. *Journal of Advances in Modeling Earth Systems* 9(1), 536–547.
- 1546       Smith, N. G., S. L. Malyshev, E. Shevliakova, J. Kattge, and J. S. Dukes
- 1547       (2016). Foliar temperature acclimation reduces simulated carbon sensitivity
- 1548       to climate. *Nature Climate Change* 6(4), 407–411.

- 1549** Soil Survey Staff (2022). Web Soil Survey. *Natural Resources Conservation Ser-*  
**1550** *vice, United States Department of Agriculture, Available online at the fol-*  
**1551** *lowing link: <http://websoilsurvey.sc.egov.usda.gov/>. Accessed 11/18/2022.*
- 1552** Soudzilovskaia, N. A., J. C. Douma, A. A. Akhmetzhanova, P. M. van Bode-  
**1553** gom, W. K. Cornwell, E. J. Moens, K. K. Treseder, and J. H. C. Cornelissen  
**1554** (2015). Global patterns of plant root colonization intensity by mycorrhizal  
**1555** fungi explained by climate and soil chemistry. *Global Ecology and Biogeog-*  
**1556** *raphy* 24(3), 371–382.
- 1557** Sulman, B. N., E. Shevliakova, E. R. Brzostek, S. N. Kivlin, S. L. Malyshev,  
**1558** D. N. L. Menge, and X. Zhang (2019). Diverse mycorrhizal associations  
**1559** enhance terrestrial C storage in a global model. *Global Biogeochemical Cy-*  
**1560** *cles* 33(4), 501–523.
- 1561** Sweet, S. K., D. W. Wolfe, A. DeGaetano, and R. Benner (2017). Anatomy  
**1562** of the 2016 drought in the Northeastern United States: Implications for  
**1563** agriculture and water resources in humid climates. *Agricultural and Forest*  
**1564** *Meteorology* 247, 571–581.
- 1565** Taylor, B. N. and D. N. L. Menge (2018). Light regulates tropical symbiotic  
**1566** nitrogen fixation more strongly than soil nitrogen. *Nature Plants* 4(9), 655–  
**1567** 661.
- 1568** Terrer, C., S. Vicca, B. D. Stocker, B. A. Hungate, R. P. Phillips, P. B. Reich,  
**1569** A. C. Finzi, and I. C. Prentice (2018). Ecosystem responses to elevated  
**1570**  $\text{CO}_2$  governed by plant–soil interactions and  
**1571** the cost of nitrogen acquisition. *New Phytologist* 217(2), 507–522.
- 1572** Thomas, R. Q., E. N. J. Brookshire, and S. Gerber (2015). Nitrogen limita-

- 1573        tion on land: how can it occur in Earth system models? *Global Change*  
1574        *Biology* 21(5), 1777–1793.
- 1575        Thomas, R. Q., S. Zaehle, P. H. Templer, and C. L. Goodale (2013). Global pat-  
1576        terns of nitrogen limitation: confronting two global biogeochemical models  
1577        with observations. *Global Change Biology* 19(10), 2986–2998.
- 1578        Thornton, P. E., J.-F. Lamarque, N. A. Rosenbloom, and N. M. Mahowald  
1579        (2007). Influence of carbon-nitrogen cycle coupling on land model response  
1580        to CO<sub>2</sub> fertilization and climate variability. *Global Biogeo-*  
1581        *chemical Cycles* 21(4), GB4018.
- 1582        Tingey, D. T., D. L. Phillips, and M. G. Johnson (2000). Elevated CO<sub>2</sub> and  
1583        conifer roots: effects on growth, life span and turnover. *New Phytolo-*  
1584        *gist* 147(1), 87–103.
- 1585        Uselman, S. M., R. G. Qualls, and R. B. Thomas (2000). Effects of increased  
1586        atmospheric CO<sub>2</sub>, temperature, and soil N availability on  
1587        root exudation of dissolved organic carbon by a N-fixing tree (*Robinia*  
1588        *pseudoacacia* L.). *Plant and Soil* 222, 191–202.
- 1589        van Diepen, L. T. A., E. A. Lilleskov, K. S. Pregitzer, and R. M. Miller (2007).  
1590        Decline of arbuscular mycorrhizal fungi in northern hardwood forests ex-  
1591        posed to chronic nitrogen additions. *New Phytologist* 176(1), 175–183.
- 1592        Viet, H. D., J.-H. Kwak, K.-S. Lee, S.-S. Lim, M. Matsushima, S. X.  
1593        Chang, K.-H. Lee, and W.-J. Choi (2013). Foliar chemistry and tree ring  
1594         $\delta^{13}\text{C}$  of *Pinus densiflora* in relation to tree growth  
1595        along a soil pH gradient. *Plant and Soil* 363(1-2), 101–112.

- 1596 Vitousek, P. M., K. Cassman, C. C. Cleveland, T. Crews, C. B. Field, N. B.  
 1597 Grimm, R. W. Howarth, R. Marino, L. Martinelli, E. B. Rastetter, and  
 1598 J. I. Sprent (2002). Towards an ecological understanding of biological nitro-  
 1599 gen fixation. In *The Nitrogen Cycle at Regional to Global Scales*, pp. 1–45.  
 1600 Springer Netherlands.
- 1601 Vitousek, P. M. and R. W. Howarth (1991). Nitrogen limitation on land and in  
 1602 the sea: How can it occur? *Biogeochemistry* 13(2), 87–115.
- 1603 Vitousek, P. M., S. Porder, B. Z. Houlton, and O. A. Chadwick (2010).  
 1604 Terrestrial phosphorus limitation: mechanisms, implications, and nitro-  
 1605 gen–phosphorus interactions. *Ecological Applications* 20(1), 5–15.
- 1606 Walker, A. P., A. P. Beckerman, L. Gu, J. Kattge, L. A. Cernusak, T. F.  
 1607 Domingues, J. C. Scales, G. Wohlfahrt, S. D. Wullschleger, and F. I. Wood-  
 1608 ward (2014). The relationship of leaf photosynthetic traits -  $V_{cmax}$  and  $J_{max}$   
 1609 - to leaf nitrogen, leaf phosphorus, and specific leaf area: a meta-analysis  
 1610 and modeling study. *Ecology and Evolution* 4(16), 3218–3235.
- 1611 Wang, H., I. C. Prentice, T. F. Keenan, T. W. Davis, I. J. Wright, W. K.  
 1612 Cornwell, B. J. Evans, and C. Peng (2017). Towards a universal model for  
 1613 carbon dioxide uptake by plants. *Nature Plants* 3(9), 734–741.
- 1614 Wang, W., Y. Wang, G. Hoch, Z. Wang, and J. Gu (2018). Linkage of root mor-  
 1615 phology to anatomy with increasing nitrogen availability in six temperate  
 1616 tree species. *Plant and Soil* 425(1-2), 189–200.
- 1617 Weatherburn, M. W. (1967). Phenol-hypochlorite reaction for determination of  
 1618 ammonia. *Analytical Chemistry* 39(8), 971–974.

- 1619** Westerband, A. C., I. J. Wright, V. Maire, J. Paillassa, I. C. Prentice, O. K.  
**1620** Atkin, K. J. Bloomfield, L. A. Cernusak, N. Dong, S. M. Gleason, C. Guil-  
**1621** herme Pereira, H. Lambers, M. R. Leishman, Y. Malhi, and R. H. Nolan  
**1622** (2023). Coordination of photosynthetic traits across soil and climate gradi-  
**1623** ents. *Global Change Biology* 29(3), 1–29.
- 1624** Wieder, W. R., C. C. Cleveland, W. K. Smith, and K. Todd-Brown (2015).  
**1625** Future productivity and carbon storage limited by terrestrial nutrient avail-  
**1626** ability. *Nature Geoscience* 8(6), 441–444.
- 1627** Wieder, W. R., D. M. Lawrence, R. A. Fisher, G. B. Bonan, S. J. Cheng, C. L.  
**1628** Goodale, A. S. Grandy, C. D. Koven, D. L. Lombardozzi, K. W. Oleson,  
**1629** and R. Q. Thomas (2019). Beyond static benchmarking: using experimental  
**1630** manipulations to evaluate land model assumptions. *Global Biogeochemical*  
**1631** *Cycles* 33(10), 1289–1309.
- 1632** Wright, I. J., P. B. Reich, and M. Westoby (2003). Least-cost input mixtures  
**1633** of water and nitrogen for photosynthesis. *The American Naturalist* 161(1),  
**1634** 98–111.
- 1635** Wright, I. J., P. B. Reich, M. Westoby, D. D. Ackerly, Z. Baruch, F. Bongers,  
**1636** J. Cavender-Bares, T. Chapin, J. H. C. Cornelissen, M. Diemer, J. Flexas,  
**1637** E. Garnier, P. K. Groom, J. Gulias, K. Hikosaka, B. B. Lamont, T. Lee,  
**1638** W. Lee, C. Lusk, J. J. Midgley, M.-L. Navas, Ü. Niinemets, J. Oleksyn,  
**1639** N. Osada, H. Poorter, P. Poot, L. Prior, V. I. Pyankov, C. Roumet, S. C.  
**1640** Thomas, M. G. Tjoelker, E. J. Veneklaas, and R. Villar (2004). The world-  
**1641** wide leaf economics spectrum. *Nature* 428(6985), 821–827.
- 1642** Xu-Ri and I. C. Prentice (2017). Modelling the demand for new nitrogen fixation

- 1643 by terrestrial ecosystems. *Biogeosciences* 14(7), 2003–2017.
- 1644 Zaehle, S., S. Sitch, B. Smith, and F. Hatterman (2005). Effects of parame-  
1645 ter uncertainties on the modeling of terrestrial biosphere dynamics. *Global*  
1646 *Biogeochemical Cycles* 19(3), GB3020.
- 1647 Zhu, Q., W. J. Riley, J. Tang, N. Collier, F. M. Hoffman, X. Yang, and G. Bisht  
1648 (2019). Representing nitrogen, phosphorus, and carbon interactions in the  
1649 E3SM land model: development and global benchmarking. *Journal of Ad-*  
1650 *vances in Modeling Earth Systems* 11(7), 2238–2258.
- 1651 Ziegler, C., M. E. Dusenage, B. Nyirambangutse, E. Zibera, G. Wallin, and  
1652 J. Uddling (2020). Contrasting Dependencies of Photosynthetic Capacity  
1653 on Leaf Nitrogen in Early- and Late-Successional Tropical Montane Tree  
1654 Species. *Frontiers in Plant Science* 11, 1–12.
- 1655 Ziehn, T., J. Kattge, W. Knorr, and M. Scholze (2011). Improving the pre-  
1656 dictability of global CO<sub>2</sub> assimilation rates under climate change. *Geophys-*  
1657 *ical Research Letters* 38(10), L10404.